Investigation on crystallographic and thermoelectric properties of poly-crystalline germanium-on-insulator substrates

静岡大学博士論文

INVESTIGATION ON CRYSTALLOGRAPHIC AND THERMOELECTRIC PROPERTIES OF POLY-CRYSTALLINE GERMANIUM-ON-INSULATOR SUBSTRATES

SELVARAJ SHANTHI

大学院自然科学系教育部

2018 年 6 月

Abstract

In recent years, thermoelectric conversion techniques have gained attention due to their potential for overcoming the energy and environmental issues. However, the thermoelectric power generator does not have sufficient conversion efficiency for practical use. The efficiency of power generator monotonously increases with increasing the thermoelectric figure-of-merit that is proportional to electrical conductivity and square of seebeck coefficient and inversely proportional to thermal conductivity. For enhancing the performance of thermoelectric power generator, the introduction of nanostructures, such as nanowires, has been expected and widely investigated since the carrier confinement effect can rise the seebeck coefficient and the phonon confinement effect leads to the reduction of the thermal conductivity.

As a thermoelectric nanostructure, group-IV semiconductors, Si, Ge, and SiGe are focused to be well defined by ultra-large scale integrated-circuit technology and compatible to Si-based devices. Thin Si-, Ge-, and SiGe-on-insulator (SOI, GOI, and SGOI) layers are required to enable the formation of patterned nanostructures on a substrate. We have focused on Ge as a thermoelectric material since crystalline Ge (c-Ge) has higher electron and hole mobility and lower thermal conductivity compared with crystalline Si (c-Si). Also, Ge crystallization in oxide matrix is thought-provoking without using the catalyst, owing to the possibility of easy oxidation. Hence, for the fabrication of thin GOI layer, the metal-induced crystallization (MIC) with catalytic metals, such as Au, Cu, and Al, is a distinguished technique of conversion of amorphous Ge (a-Ge) into c-Ge. Henceforth, it is essential to investigate the thermoelectric characteristics of poly-Ge on insulator substrates. For this study, bilayer thin films of metal catalyst/a-Ge were taken as a starting structure.

The main objective of this research is (1) to fabricate the poly-Ge on insulator substrates using the metal-induced crystallization (MIC) with the effect of catalytic metals, such as Au, Cu, and Al. (2) To analyses the crystallographic and thermoelectric characteristics of poly-Ge on insulator substrates. In order to avoid the alloy formation, the annealing conditions were performed with reference to the corresponding eutectic temperature of Ge with the metals Au, Cu and Al.

Ge crystallization of Au induced crystallization was performed around the eutectic temperature of Ge-Au mixture at 300 ºC, 400 ºC and 500 ºC for 60 min, for the starting structure of metal catalyst Au (20nm)/a-Ge (100nm), using the conventional furnace annealing process. Ge crystallization of Cu induced crystallization was performed at 400 ºC for 4 hours, which is lower than the eutectic mixture of Ge-Cu. The annealing process of conventional furnace and rapid thermal were discussed for the starting structure of metal

catalyst Cu (20nm)/a-Ge (100nm). Ge crystallization of Al induced crystallization was performed at 350 ºC for 2 and 4 hours, which is lower than the eutectic mixture of Ge-Al, using rapid thermal annealing process for the starting structure of metal catalyst Al (100nm)/a-Ge (100nm).

XRD (X-Ray Diffraction) and Raman analysis revealed that the poly-Ge were formed on the insulator substrates, with the effect of catalytic metals. Microscopic (FE-SEM, Field Electron- Scanning Electron Microscopy and Optical microscopy) analysis signified that the poly-Ge were formed as an island like layer over the entire substrate. FE-EPMA (Field Electron-Electron Probe Micro Analyzer) analysis implied the Ge distribution with corresponding positions of Si, O and metal catalysts with lower detectable limits. EBSD (Electron Backscattering Detector) analysis clarified the formation of dominant (111)-oriented poly-Ge on insulator substrates. XPS (X-ray Photoelectron Spectroscopy) analysis elucidated the formation of elemental Ge spectra during the Ge crystallization process.

Thermoelectric characteristics of seebeck coefficient and thermal conductivity analysis were performed. The measured seebeck coefficients were scattered and no significant difference was achieved for the Ge layer, with and without the influence of metal catalyst. It was reported that few metal atoms left over in the Ge layer acted as a (dopant) carrier source to control the carrier concentration values. For the thermal conductivity analysis, it was found that the crystallized Ge film with the influence of metal catalysts has larger thermal conductivity than the Ge film formed without the influence of metal catalyst. The increase in the thermal conductivity of the MIC-formed Ge film was considered to originate from the crystallization of the Ge film, taking account of the result that the Ge layer contains few metal atoms and the fact that the thermal conductivity in a crystal material is usually larger than that in an amorphous material.

Acknowledgements

My Ph.D. would not have been possible without getting the financial support from prestigious Japanese Government scholarship MEXT.

I owe my sincere thanks to Double Doctoral Program (DDP) of SRM University, India in collaboration with Shizuoka University, Japan. I have been accomplished a big deal of both research studies and life, in general.

I am obligated to my supervisor Prof. Dr. Hiroya Ikeda, and Prof. Dr. Yasuhiro Hayakawa, Research Institute of Electronics, Shizuoka University, Japan for giving their endless support to me to achieve my career goal and always with me during my harder times. I am grateful to Dr. Yosuke Shimura, Research Institute of Electronics, Shizuoka University, Japan for giving his valuable suggestions during the project discussions.

I am thankful to Prof. Dr. Kenji Murakami, Director, Centre for Nanodevice and Joint research laboratory, Shizuoka University, Japan for permitting me to carry out my instrumental analysis. I have worked with the technicians Mr. Tomoda Waichi, Mr. Koyama Tadanobu, Mr. Mizuno Takeshi, and Mr. Makamoto Ishikawa from Shizuoka University, Japan during my doctoral studies. They helped me in learning the nook and corner of the instruments.

I am indebted to another supervisor Prof. Dr. Muthamizhchelvan Chellamuthu, SRM University, India for giving this wonderful opportunity to pursue my doctoral studies at Shizuoka University, Japan. I would like to express my deep acknowledgement to Prof. Dr. S. Ponnusamy, SRM University, India for his support throughout my doctoral studies at Shizuoka University, Japan.

Most importantly, I wish to thank my parents Mr. V. Selvaraj, Mrs. S. Umamaheswari and my brother Mr. S. Vignesh Kumar for their unconditional love and patience.

Finally, I thank lord almighty for his countless blessings.

Table of contents

List of Figures

Chapter 1: Introduction

1.1 Germanium-Device for future electronics

Group IV semiconductors Silicon (Si) and Germanium (Ge) are the exclusive materials owing to their semiconducting, electrical, optical properties in the field of micro and nano devices[1-3]. Compared with the conventional Si materials, Ge[4] has several unique properties such as larger dielectric constant, smaller carrier mass. Future electronics mainly deals with the choice of material as Germanium (Ge), due to its significant advantages in the application of thin film transistors[5], photovoltaic solar cells[6], lithium-ion battery[7] etc., Particularly, polycrystalline (pc)-Ge may be a potential material that can replace polycrystalline-Si (pc-Si), owing to its higher carrier mobility[8,9,10] and intrinsic electronic conductivity compared to Si, due to its smaller band gap[11]. Hence, it is essential to expand the study on the transformation of a-Ge to crystallization of Ge.

At a nanometer scale, a grain of poly-crystalline Ge can be acts as a single crystal, in achieving the high mobility independent of grain boundaries. It initiates the way to fabricate the high-quality poly-crystalline Ge at a low-temperature process for utilizing the applications in the fields of logic and photonic devices[12].

1.2 Metal Induced Crystallization process

Low-temperature formation of pc-Ge can be achieved using the crystal growth techniques including metal induced crystallization, laser annealing[13], and chemical vapor deposition[14]. Metal-induced crystallization (MIC) is one of the notable mechanism of conversion of an amorphous form of

semiconductors (a-Si, a-Ge, a-SiGe) into crystalline form (c-Si, c-Ge, c-SiGe) with the influences of catalytic metals like Au, Al, Ag, Ni etc.,[15-29].

Fig. 1.1 represents the schematic diagram of the metal induced crystallization process. Initially, a catalytic metal is deposited over the substrate. Then, the amorphous form of Ge (a-Ge) is deposited over the catalytic metal/ substrate. Now the substrate is subjected to the annealing process to undergo the metal induced crystallization process. After the removal of metal residues contamination, poly-crystalline Ge is achieved.

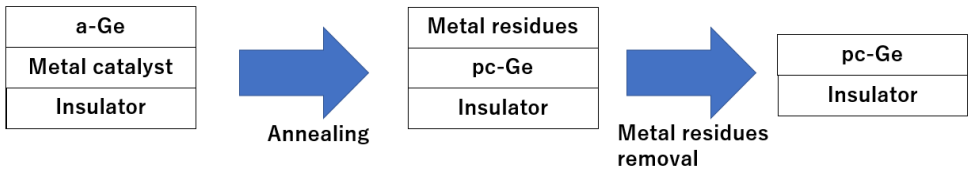

Fig. 1.1 Schematic diagram of metal induced crystallization process.

1.3 Furnace annealing process

Annealing process is the major key to carry out the crystallization. It includes the conventional furnace annealing (CFA) and rapid thermal annealing (RTA) process. While comparing with the CFA process, RTA process has a high degree of crystallization. Also, RTA[30] has been considered as the primary annealing technique in the semiconductor industry to achieve the better crystallization results. RTA process includes three phases namely, rising temperature phase, holding temperature phase and cooling phase. Usually, the nucleation process will take place in the rising temperature phase. During this stage, nuclei are formed on a large scale over the substrate and then the holding temperature phase starts to perform the crystal growth. Then the final phase of cooling will take place. In contrast, for the CFA process, the nucleation phase takes a longer time to form the lower number of nuclei over the substrate. Holding time of CFA is not as much

effective as RTA process, then finally, cooling phase takes longer time than the RTA process. During the annealing process, Si and Ge are subjected to stress factor due to thermal expansion. It is defined as the tendency of materials subjected to change in its shape, area and volume with corresponding to change in temperature. The linear co-efficient of thermal expansion for SiO_2 and Ge is represented as 0.5 x 10^{-6} K^{-1} and 5.8 x 10^{-6} K^{-1}.

1.4 Thermoelectric characteristics of poly -crystalline Ge

The three important factors to be considered for the good thermoelectric materials are Seebeck coefficient, S, electrical conductivity, σ, and thermal conductivity, k. Thus, the efficiency of a thermoelectric module is determined by the dimensionless figure of merit, $z= ((S^2 \sigma)/ k) T$. In the above relation T is denoted as the absolute temperature. In order to achieve the high efficiency of thermoelectric devices, the seebeck coefficient must be high or the thermal conductivity value should be low. Now the achieved value of ZT is 1, which is very low and hence the efficiency of the device should be reduced. Hence, the main objective is to enhance the ZT value to enhance the thermoelectric device performance. Considering the nanostructures are one the main key factors to enhance the ZT, by lowering the thermal conductivity values with the increase in seebeck coefficient values.

1.5 Outline of the thesis

Chapter 1 defines the introduction of poly-crystalline Germanium for the thermoelectric applications. It also clearly describes the motivation of this study.

Chapter 2 is a brief introduction to Germanium thin film deposition of Vacuum thermal evaporation technique. Characterization analysis of Microstructure and thermoelectric measurements are clearly elucidated with the specification of the instruments.

Chapter 3 designates the fabrication of Gold (Au) induced crystallization of amorphous

Germanium on SiO_2/Si substrate, using the conventional furnace annealing (CFA) around the eutectic temperature of Au-Ge for 60 min. Microstructure and thermoelectric characterizations of the poly-crystalline Germanium islands on SiO_2/Si substrate are analyzed.

Chapter 4 reports the investigation of Copper (Cu) induced crystallization of amorphous Germanium on SiO_2/Si substrate. Annealing methods of conventional furnace annealing (CFA) and rapid thermal annealing (RTA) are employed at a lower eutectic temperature of Cu-Ge for 4 hours to achieve the uniform poly-crystalline Germanium thin layer on SiO_2/Si substrate. Also, the investigation of microstructure and thermoelectric characterizations of poly-crystalline Germanium thin layer on SiO_2/Si substrate are studied.

Chapter 5 presents the examination of rapid thermal annealing (RTA) of Aluminum (Al) induced crystallization of amorphous Germanium on SiO_2/Si substrate at a lower eutectic temperature of Al-Ge for 2 and 4 hours. Islands of poly-crystalline Germanium and porous structure of Poly-crystalline Germanium on SiO_2/Si substrates are achieved during the annealing process and its characterization analysis of microstructure and thermoelectric measurements are investigated.

Chapter 6 concludes with a summary of the key achievements of the dissertation, and future directions.

Chapter 2: Growth and characterization of Germanium thin films

2.1 Growth of Germanium thin films

In the semiconductor industry, many research experiments have been done so far to grow the high-quality crystalline Ge-on-insulators (GOI) substrates. In this work, Physical Vapor Deposition[31,32] (PVD) techniques have been implemented to develop the amorphous Germanium thin films on insulator substrates. PVD is the method of depositing the source material on to the target substrate by physical means. Usually, the thickness of the deposition thin film ranges from few nm to μm. This technique is environmentally friendly since the deposition process mainly takes place inside the vacuum chamber. It mainly falls into two categories namely thermal vapor evaporation and sputtering technique. In this study, all the deposition process has been done with the thermal vapor evaporation system.

2.1.1 Vacuum deposition technique of Germanium thin films

Evaporation[33] is the simplest PVD technique to develop the thin film layers on the substrate. The main constituents of this thermal vapor deposition system consist of evaporation vacuum chamber with vacuum gauge monitor, electrical power output and input system, discharge and rotary pump, cooling machine, source material, target substrate, thickness monitor-sensor set up, liquid Nitrogen inlet. During the thermal evaporation process, the electrical voltage input to the system melts the source material that vaporizes towards the target substrate in the evaporation vacuum chamber. Thickness sensor place inside the evaporation vacuum chamber signifies the thickness value in the thickness monitoring set up box, which

is placed outside. Vacuum gauge set up is necessary to maintain the vacuum pressure of 6.0 x 10^{-4} Pa, while in operation.

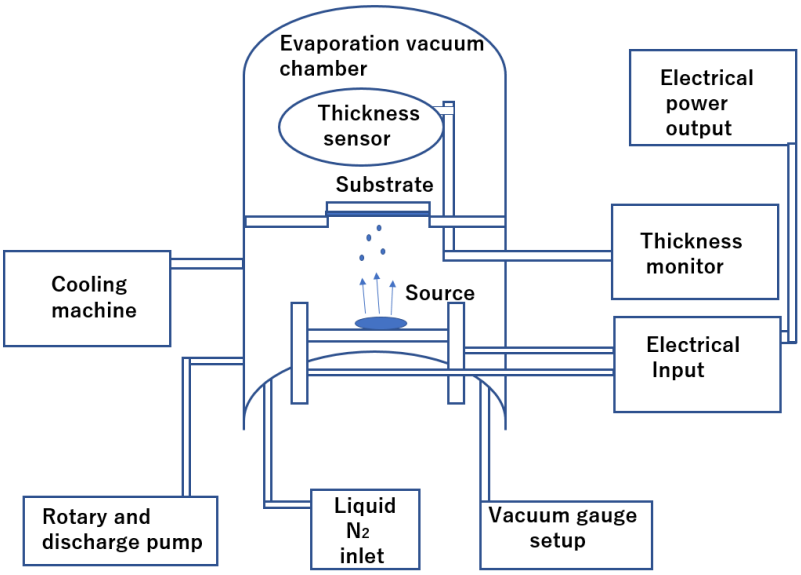

Figure 2.1 Typical line diagram of thermal vapor deposition system.

Throughout the operation, liquid N_2 should be replenished to the thermal vapor evaporation system with one-hour interval. Fig. 2.1 represents the typical line diagram of thermal vapor deposition system. When increasing the electrical input voltage to the thermal vapor evaporation system to melt the source material, it is advised to switch on the cooling machine to avoid the unnecessary problem which can affect the deposition process.

2.2 Microstructure Characterization Analysis

The microstructure characteristics of the as-deposited and annealed Ge thin films were characterized using the following techniques. The structural appearance of the as-deposited and annealed samples was observed using optical digital microscope (KH-8700, Hirox). The surface morphology of the samples was examined, using field-emission scanning electron microscopy (FE-SEM; JSM-7001F, JEOL, Japan). Raman spectroscopy measurements were performed at room temperature, using New Raman

Spectrometer (NRS-7100) with a laser excitation wavelength of 532nm, spot size 1µm. The elemental mapping and line profile analysis were analyzed using field emission scanning electron microscopy (FE-SEM; JSM-6335F, JEOL, Japan) and electron probe micro analyzer (EPMA-JXA-8530, JEOL, Japan). The crystal structure of the samples is evaluated using a*n* X-ray diffractometer (XRD, RINT-2200 diffractometer, Rigaku, Japan, CuKα radiation, λ=1.54178 Å). The crystal orientation was analyzed by electron backscattered diffraction (EBSD) analysis, field emission scanning electron microscopy (FE-SEM; JSM-7001F, JEOL, Japan). The chemical bonding of the sample surfaces was identified through x-ray photoelectron spectroscopy (XPS; Shimadzu ESCA 3100).

2.3 Thermoelectric characteristics of Germanium thin films

The main purpose of this study was the investigation of thermoelectric characteristics of the Ge thin film on insulator substrates, it was essential to examine the seebeck coeffiecient and thermal conductivity analysis of the Ge-on- insulator (GOI) substrates. This study did not include the electrical characteristics, since the Ge-on- insulator (GOI) substrates failed to attain the minimum voltage to perform the electrical studies. In this study, all the thermoelectric characteristics of the Ge-on-insulator substrates were performed at room temperature.

2.3.1 Seebeck coefficient measurement

For measuring the seebeck coefficient analysis, Ge-on-insulator substrates were deposited with pt electrodes at both the ends to form the ohmic contact. Fig 2.2 signifies the schematic diagram of photodetectors with metal contacts to perform the thermoelectric operations.

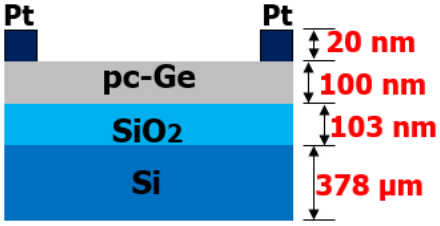

Fig 2.2 Schematic diagram of photodetectors with metal contacts.

The Seebeck coefficient was measured at room temperature after forming Pt electrodes, using a conventional method[34,35]. Fig. 2.3 represents the schematic diagram of seebeck coeffiecient measurement setup of Ikeda laboratory. Resistive heaters were placed under the copper plates, which were placed horizontally with a gap of 1 mm in a shield box. The sample was placed in contact with the two copper plates. Each resistive heater placed under the copper plates were heated independently. Hence, a temperature difference could be obtained in a plane parallel to the sample surface, by controlling the current to the resistive heaters. Two K-type thermocouples along with a couple of probes were directly connected to the sample surface.

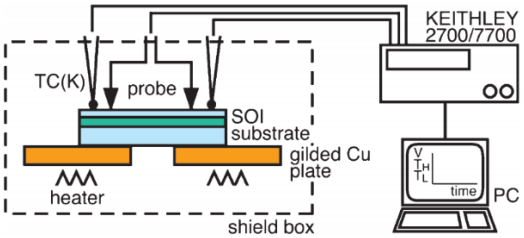

Figure 2.3 Typical line diagram of seebeck coeffient measurement setup[34].

The corresponding changes at the high- and low- temperature regions with the changing time of the thermoelectricmotive force was measured using a digital multimeter (Keithley 2700) equipped with a switching module (Keithley 7700). The seebeck coefficient is defined as the ratio of thermoelectric force ($\triangle V= V_H -V_L$) to the temperature difference ($\triangle T= T_H -T_L$).

2.3.2 Thermal conductivity analysis

The thermal conductivity analysis of the Ge-on-insulator substrates was performed using the picosecond time-domain thermoreflectance (TDTR) method[36,37]. Prior to the thermal conductivity measurement analysis, a thin layer of Molybdenum (Mo) with the thickness 100nm was deposited on the surface of the Ge-on-insulator substrates, to reflect the laser source from the surface. Fig. 2.4 shows

the line diagram of thermal conductivity analysis measurement model. It consists of laser source, optical system and monitoring display. The optical system is the main unit, where the overall thermal conductivity measurement analysis was performed. The cross-sectional thermal conductivity of the Ge-on-insulator substrates was measured by the front-heating front-detection method of TDTR. Fig. 2.5 represents the estimation equation of front-heating front-detection method. In evaluating the thermal conductivity from the thermal effusivity, the specific heat capacity 323 $Jkg^{-1}K^{-1}$ and the density 5324 kgm^{-3} were used for Ge.

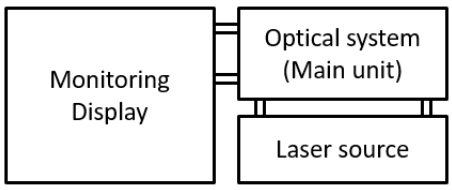

Figure 2.4 Line diagram of front- heating front-detection method of the Ge-on-insulator substrates.

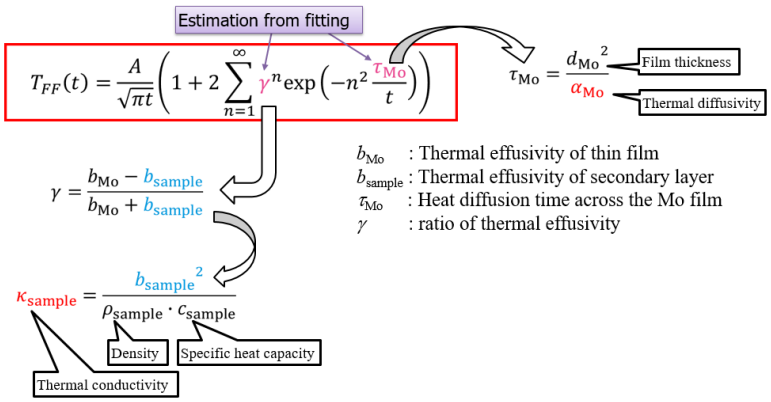

Figure 2.5 Estimation equation of front-heating front-detection method.

The above stated microstructure characterization of Optical microscopy, X-ray diffraction (XRD) analysis, Raman, Field Emission Scanning Electron Microscopy (FE-SEM), Field Emission Electron Probe Micro Analyzer (FE-EPMA), Electron back scattering diffraction(EBSD) analysis and X-ray Photoelectron Spectroscopy (XPS), and thermoelectric characterizations including seebeck coefficient and thermal conductivity measurement analysis were investigated during this study.

Chapter 3: Polycrystalline Germanium thin films: Au induced crystallization of a-Ge

3.1 Background of Au induced crystallization of a-Ge thin films

Many works have been widely studied for achieving the pc-Ge thin films on insulators, using Au induced crystallization of a-Ge at low temperature[38-42]. Predominantly, the crystallization process using Au as a catalyst is gaining interest, with respect to the crystalline quality and electrical properties[43]. Similarly, the Au catalyst strongly influences the particle size formation, with reference to the annealing conditions[44]. In addition, semiconductor structures[45] at nanoscale regime are the key factor for the unique applications in the field of electronics, photonics and thermoelectrics[46].

The effective role of metal catalyst Au is (1) to act as a carrier source, which influence the thermoelectric properties, (2) crystallization of Si and Ge at low temperature, with the grain size varies from ten to a few tens of nanometers and (3) fine structure is important for high thermoelectric performance. In these literature reports, equal ratio of metal-semiconductor thickness was employed to induce the layer exchange mechanism of metal induced crystallization. Interestingly, Au-Ge system has lower eutectic temperature value of 361 ºC[47]. By annealing above the eutectic temperatures, crystallization is not as much as distinct. Hence, it is essential to fabricate the c-Ge, below the eutectic temperature of Ge-Au. However, in this study, the Ge crystallization was performed at 300º C, 400º C and 500º C for a shorter time of 60 min, with the starting structure of Au (20nm)/Ge (100nm). And the microstructure and thermoelectric characteristics have been investigated with and without the influence of metal catalyst Au i.e., w/Au and w/o Au.

3.2 Experimentation and sample preparation

3.2.1 Sample preparation and growth mechanism

In this study, commercially available SiO_2/Si was pre-cleaned using piranha solution for 1 min. Preparation of Au and Ge layers on SiO_2(thickness:103nm)/Si(thickness:378µm) substrate was carried out at room temperature. Initially, amorphous-Ge (a-Ge) thin layer (thickness: 100nm) was deposited on SiO_2/Si substrate, using vacuum evaporation system in a vacuum chamber with a base pressure of 6.0 x 10^{-4} Pa. Consequently, a thin layer of Au (thickness: 20nm) was deposited on a-Ge/SiO_2/Si substrate, using Au sputter. After that, the sample consists of Au/a-Ge/SiO_2/Si was subjected to conventional furnace annealing (CFA) for the Ge crystallization process, around the eutectic temperature of Ge-Au binary phase eutectic system, at 300º C, 400º C and 500º C for 60 min, in an N_2 ambient. After the completion of conventional furnace annealing process, the residual Au metal layer was etched using aqua regia for few seconds.

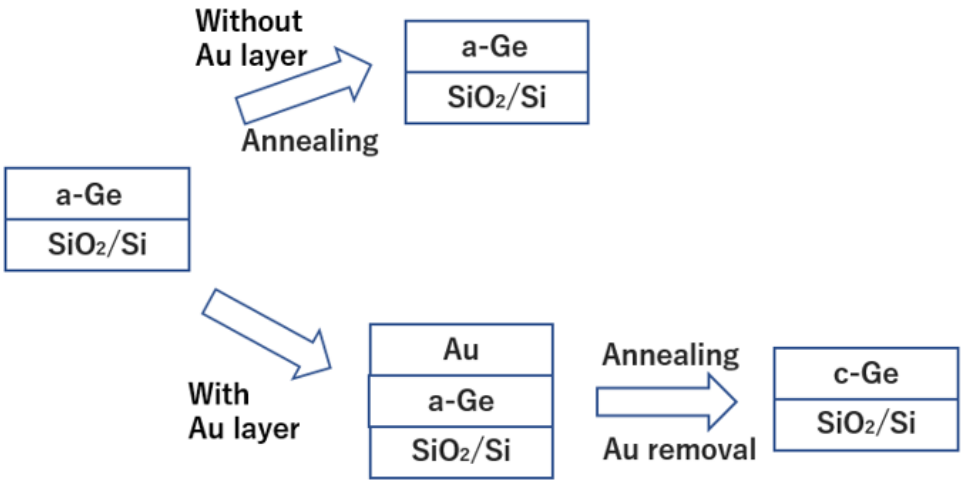

Figure 3.1 Schematic of Au-induced crystallization process of Ge film on SiO_2/Si substrate.

For reference, a-Ge/SiO_2/Si substrate was also annealed at 300º C, 400º C and 500º C for 60 min, in an N_2 ambient, to check the influence of metal catalyst Au, during the crystallization process. The experimentation process flow diagram is schematically represented in Fig.3.1. Hereafter, the Ge crystallization process without and with the influence of metal catalyst Au is represented as w/o Au and

w/Au.

Initially, the as-deposited Ge thin films were in amorphous phase. The Ge crystallization process began with the nucleation process for 30 min. During this stage, nuclei were formed with corresponding to the increase in the annealing temperature. The densification of nuclei was based on the annealing temperature of bilayer thin film. Then the Ge crystal growth process was performed at 300º C, 400º C and 500º C for a shorter time of 60 min. The Ge crystals were formed with corresponding to the increasing annealing temperature. Fig. 3.2 clearly depicted the Ge crystal growth mechanism during the conventional furnace annealing (CFA) process. The possibility of formation of Ge-Au alloy was reduced due to the shorter time of 60 min and usage of a metal catalyst with a lower ratio. Higher temperature has taken more time cooling time than lower temperature.

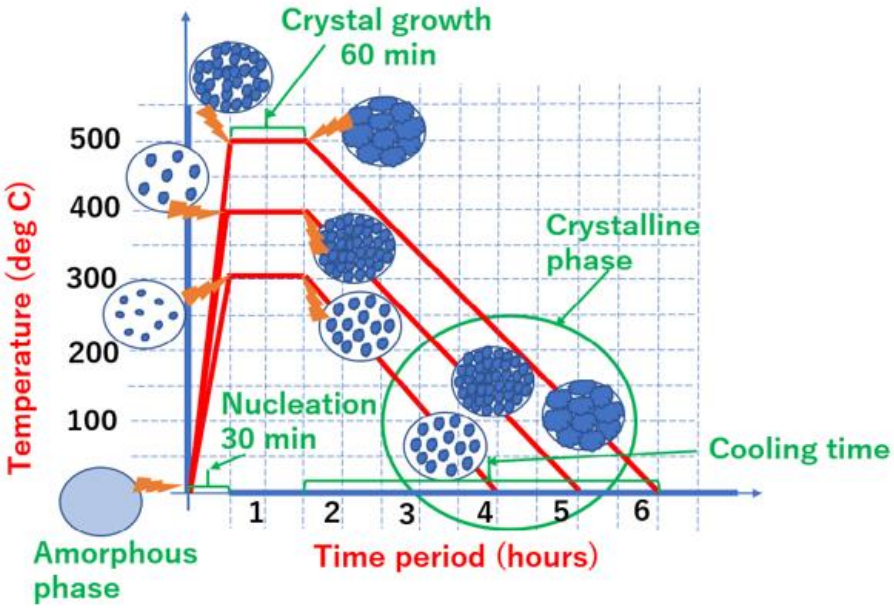

Figure 3.2 Growth mechanism of Au induced crystallization of Ge during the conventional furnace annealing (CFA) process.

3.3 Microstructure Characterization Analysis

3.3.1 Optical microscopy

Fig.3.3 shows the optical microscopy analysis of the as-deposited and annealed samples. Figs. 3.3(a)-(c) show the optical analysis of the as-deposited a-Ge/SiO_2/Si, Au/SiO_2/Si, Au/Ge/SiO_2/Si. Figs. 3.3(d)-(f) show the optical analysis of the annealed samples at 300º C, 400º C and 500º C for 60 min, without the influence of metal catalyst Au (w/o Au). Figs. 3.3(g)-(i) show the optical analysis of the annealed samples at 300º C, 400º C and 500º C for 60 min, with the influence of metal catalyst Au (w/ Au). The changes in the color appearances of the as-deposited samples represented the thin layer deposition on the SiO_2/Si substrate. For the case of samples annealed at 300º C, 400º C and 500º C for 60 min, without the influence of metal catalyst Au (w/o Au), no distinguished changes were observed. Hence, it was not possible to detect the surface appearance of the samples. Also, for samples annealed at 300º C, 400º C and 500º C for 60 min, w/ Au, it was seen that the surface appearance was changed while comparing with the previous cases of w/o Au. Other than no remark was taken into the account of Ge crystallization process.

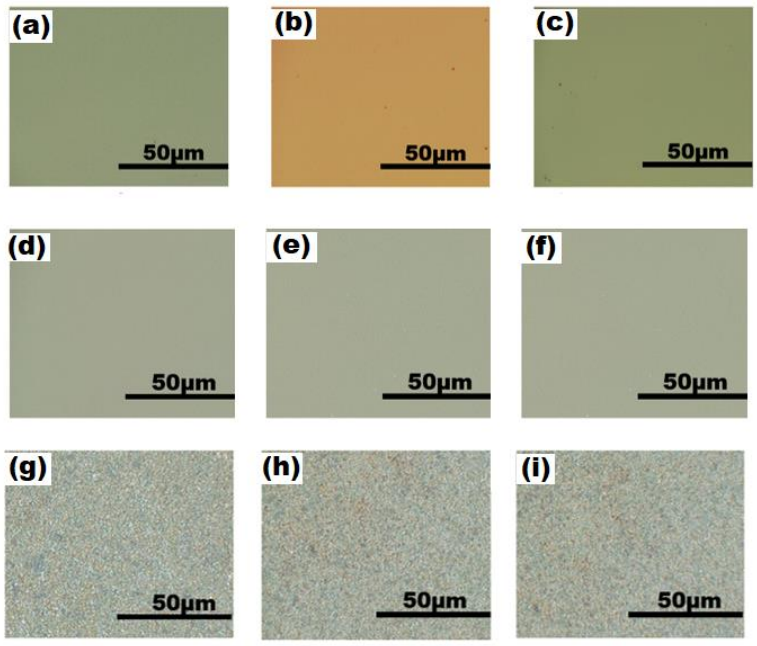

Figure 3.3 Optical microscopy image of the samples over SiO_2/Si at each stage of crystallization process. (a) a-Ge layer, (b) Au thin layer, (c) Au/a-Ge. After annealing, w/o Au layer, (d) 300 ºC, (e) 400 ºC, (f) 500 ºC. After annealing, w/Au layer, (g) 300 ºC, (h) 400 ºC, (i) 500 ºC.

3.3.2 X-Ray Diffraction (XRD)

XRD profiles of the Ge layers annealed at 300, 400 and 500 ºC for w/o Au and w/Au layer were shown in Fig. 3.4 (a) and (b). It was found that the significant peak is hardly observed in these profiles except for the Si (200) peak at ~33.4º originating from the Si substrate in Fig. 3.4(a) and (b). This result indicates that the Ge layer remains amorphous, resulting in the flat surface later observed in SEM images (Fig. 3.6). Therefore, no significant change happens without Au at these annealing temperatures. In contrast, in the XRD profiles of the Ge layers formed w/Au, (Fig. 3.4(b)), a Ge (111) peak at ~27.4º can be clearly observed even for the 300 ºC-annealed Ge layers.

Hence, it can be said that the Au catalyst plays a role of enhancing the crystallization of Ge film. The Ge (111) peak becomes more significant at annealing temperature above 400 ºC. Considering that these annealing temperatures are higher than the eutectic temperature of the Ge-Au alloy system, the crystallization of Ge seems to be enhanced due to the existence of the liquid-phase Ge.

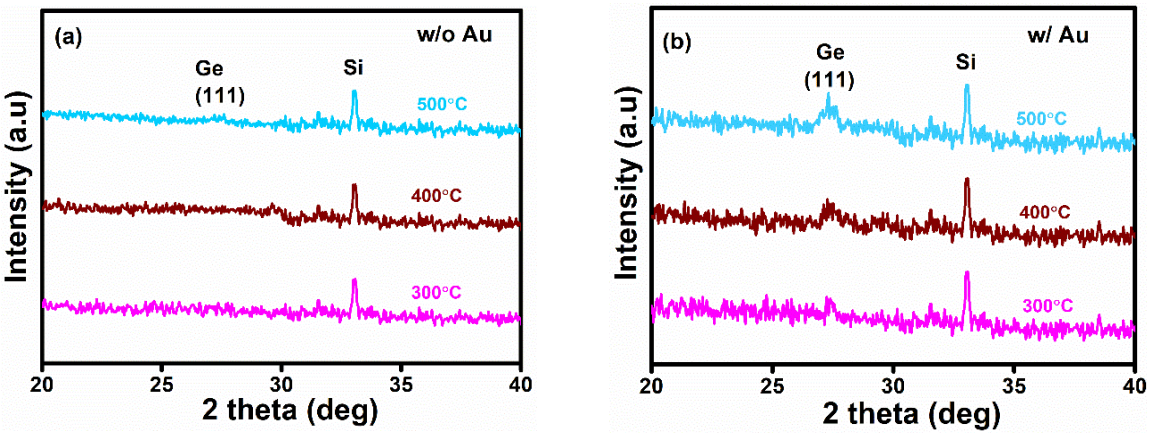

Figure 3.4 XRD profiles of annealed Ge films (a) w/o Au and (b) w/ Au.

3.3.3 Raman Spectroscopy

Fig. 3.5 (a) and (b) show Raman spectra obtained from the Ge layers annealed at 300, 400 and

500 ºC for w/o Au and w/Au layer. It was confirmed that the as-deposited Ge has a broad peak at 284 cm^{-1} corresponding to Ge-Ge bonds in a-Ge[48]. The a-Ge peak was observed in the prepared Ge layers w/o Au catalyst even after annealing at 500 ºC, as shown in Fig. 3.5(a). For the Ge layer, w/Au, in contrast, a sharp peak of Ge-Ge bond at 297 cm^{-1} was clearly observed, as shown in Fig. 3.5(b), which is assigned to c-Ge[48].

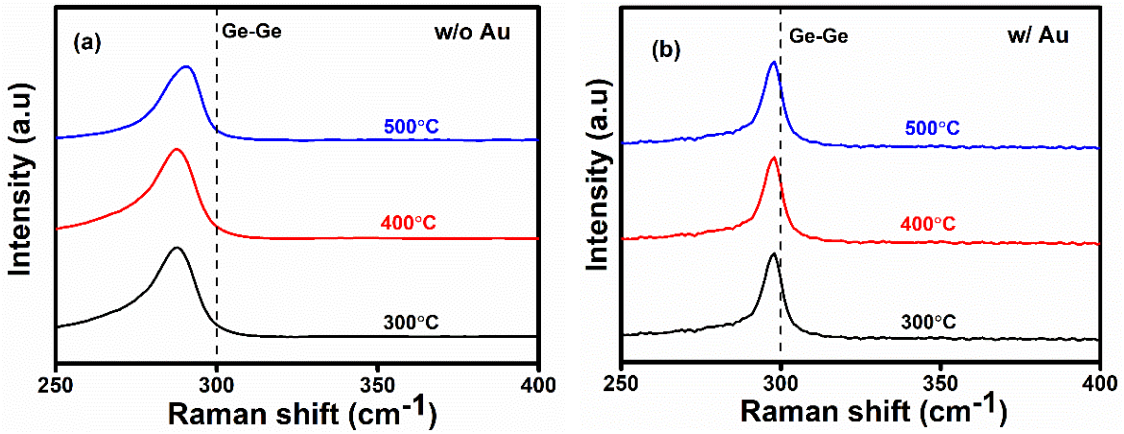

Figure 3.5 Raman spectra of annealed Ge films (a) w/o Au and (b) w/ Au.

These findings indicate that the Au catalyst makes the Ge film crystalized even at 300 ºC while the Ge film without Au is dominantly amorphous after annealing at 500 ºC, which is consistent with the other characterization results. The Ge-Ge peak position observed in the Ge film, w/Au is slightly lower than 300 cm^{-1} in bulk c-Ge. This would be due to amorphous and nano-crystalline Ge present in the layer[49]. Moreover, it was confirmed that Ge-Au component is below the detection limit in Raman spectra.

3.3.4 Field Emission-Scanning Electron Microscopy (FE-SEM)

Fig. 3.6 indicates FE-SEM images of the Ge layer surfaces after annealing at 300, 400 and 500 ºC for w/o Au and w/Au layer. While the Ge layers w/o Au catalyst seem to have a smooth surface as shown in Figs. 3.6(a)-(c), the Ge surfaces formed w/Au show bright domains in the SEM images of Figs. 3.6(d)-(f). These findings strongly suggest that the bright domains in the SEM images of Figs. 3.6(d)-(f)

correspond to Ge islands and contain few Au atoms.

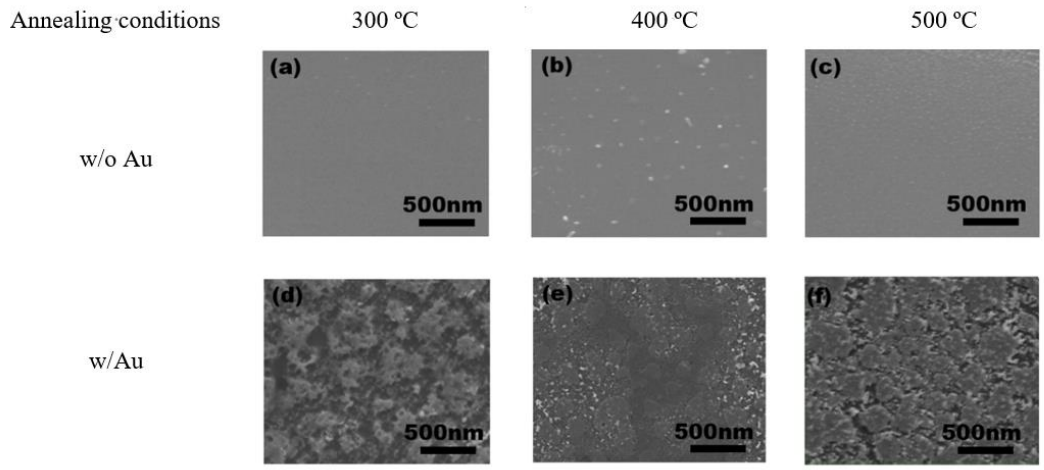

Figure 3.6 FE-SEM images of the Ge layer surfaces after annealing at 300 ºC, 400 ºC and 500 ºC for w/o Au and w/Au layer.

3.3.5 Field Emission- Electron Probe Micro (FE-EPMA)

Fig. 3.7 is EPMA images (top), elemental line profile (middle), and Ge distribution (bottom) of the GIC-formed Ge films. In the elemental line profile, obtained at a yellow line in the EPMA image, Si and O signals were observed all over the prepared layer and there was no significant difference in their amounts among the samples. These signals originated from the SiO_2/Si substrate. The Ge distribution mostly coincided with the bright domains observed in the EPMA image. The elemental line profile in the 500 ºC-annealed sample clearly indicates that the Ge intensity increases at the bright domain while the Au intensity is significantly observed at the dark regions.

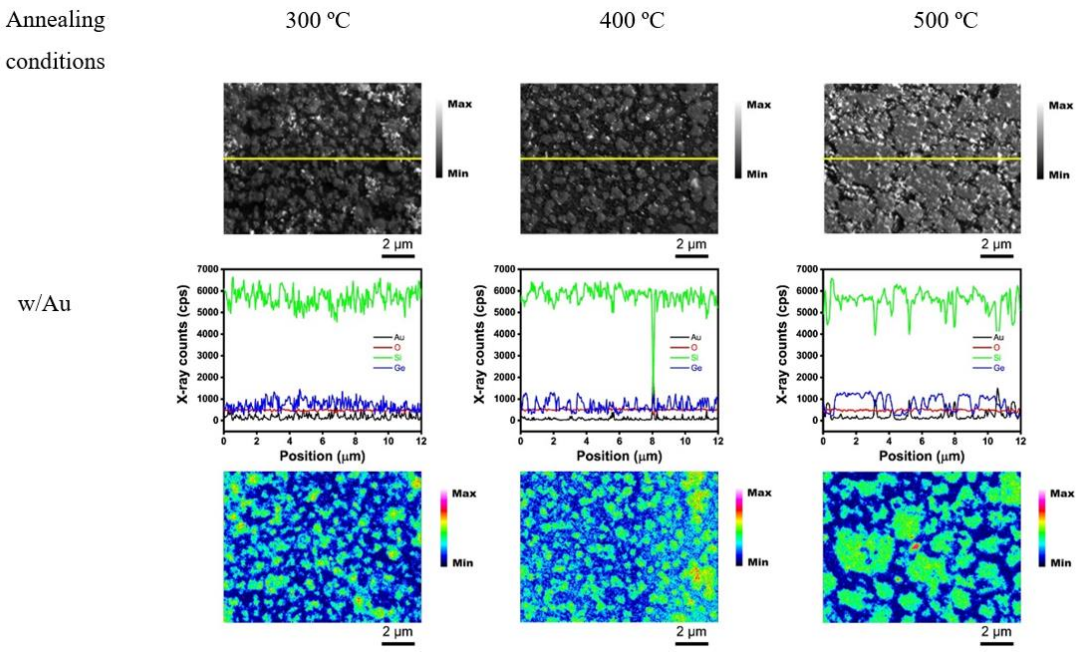

Figure 3.7 EPMA images (top), elemental line profile (middle), and Ge distribution (bottom) of GIC-formed Ge films. The line profile corresponds to the yellow line in the EPMA image. The color bar indicates intensity of Ge atom signals in the bottom images.

3.3.6 Electron Back Scattering Detector (EBSD)

Fig. 3.8 is the EBSD images of the samples annealed at (a) 300º C, (b) 400º C and (c) 500º C for 60 min, w/Au. Annealed sample at 300º C shown the poly-crystalline Ge surface with the mixed orientation. For all cases, annealing at 400º C and 500º C, Ge with dominant (111) oriented surfaces were achieved with the increasing annealing temperature of 400º C and 500º C for 60 min. Since the magnification scale of EBSD image of Ge surfaces was at 100nm, Ge islands were not clearly identified. The inset color triangle represents the corresponding orientation of the Ge surfaces. The EBSD analysis is consistent with the XRD and Raman analysis.

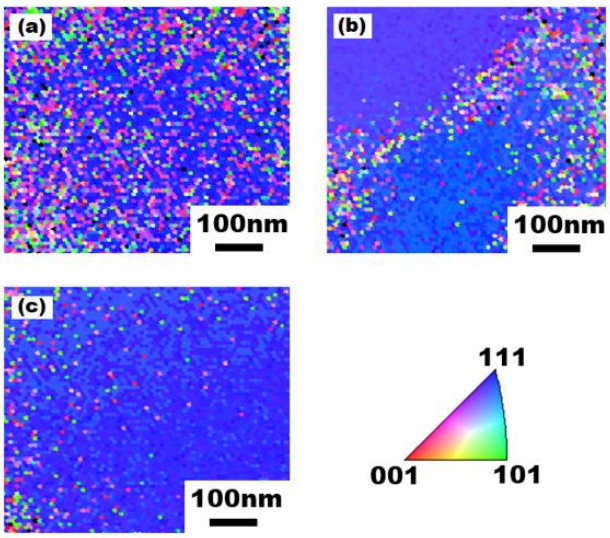

Figure 3.8 EBSD images of the samples annealed at (a) 300º C, (b) 400º C and (c) 500º C for 60 min, w/Au.

3.3.7 X-ray Photoelectron Spectroscopy (XPS)

Fig. 3.9 shows the XPS analysis of the samples (a) as-deposited a-Ge, annealed at (b) 300º C, (c) 400º C and (d) 500º C for 60 min using CFA, w/o Au and w/ Au. A high intensity peak observed at 29.5 eV, was assigned to the elemental Ge 3d spectra, as shown in Fig. 3.9 (a). From Fig. 3.9 (b), for 300 º C w/ Au, peak observed at 29.5 eV was allocated to the elemental Ge 3d spectra and for w/o Au, two peaks were observed at 29.7 and 32.4 eV were allocated to elemental and sub-oxide peak of Ge 3d spectra[69-72]. From Fig. 3.9 (c), for 400 º C w/ Au, a peak observed at 30.3 eV assigned to the sub-oxide peak of Ge 3d spectra and for w/o Au, two peaks detected at 29.9 and 33 eV, were assigned to the sub-oxide peaks of Ge 3d spectra. From Fig. 3.9 (d), for 500 º C w/ Au, a peak observed at 29.9 eV assigned to the sub-oxide peak of Ge 3d spectra and for w/o Au, peak 33.5 eV, was allocated to the sub-oxide peaks of Ge 3d spectra.

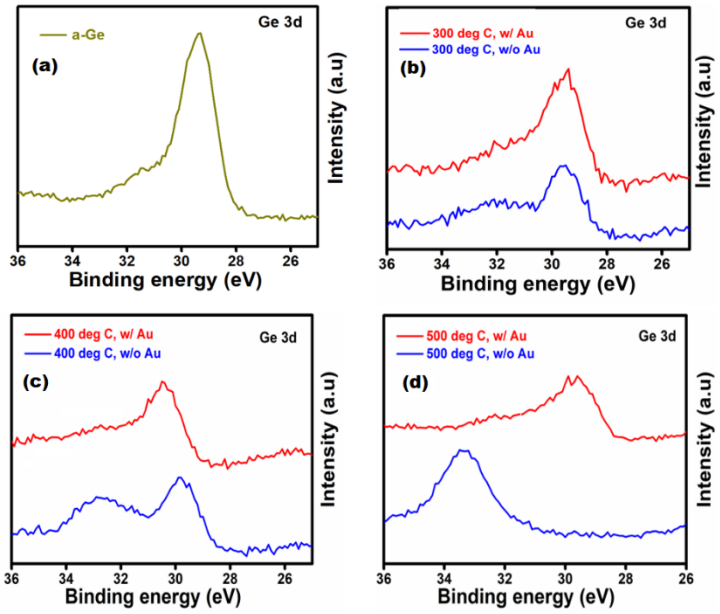

Figure 3.9 XPS analysis of the samples (a) as-deposited a-Ge, annealed at (b) 300° C, (c) 400° C and (d) 500° C for 60 min.

3.4 Thermoelectric characteristics

3.4.1 Seebeck coefficient measurement

The Seebeck coefficient of the Ge layer w/o Au and w/Au catalyst are shown in Fig. 3.10, as a function of annealing temperature. The data of the as-deposited Ge layer are also indicated in these graphs for comparison.

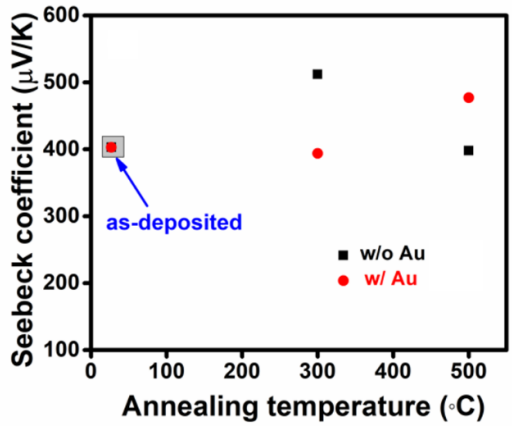

Figure 3.10 Seebeck coefficient Ge film w/o Au and w/ Au catalyst, as a function of annealing temperature.

The Seebeck coefficient for the Ge layer with (or without) Au annealed at 400 ºC could not be measured owing to its high electric resistance, which indicates a small number of carriers in the Ge layer. Although the measured Seebeck coefficients scatter in Fig. 3.10, there is not a significant difference between with and without Au catalyst. As described above, it could not be confirmed that Au makes Ge-Au bonds in the Ge film, however, even if there is Ge-Au bond, the impurity level formed in Ge energy bandgap is too deep to act as acceptor at room temperature[50]. Therefore, the Seebeck coefficient is not influenced by Au atoms. It is reported that Au atoms remain in the Ge layer and work as a carrier source in the case using repeated Au/Ge bilayers as a precursor material[51]. In this case, the carrier concentration seems difficult to be controlled because the carrier concentration is automatically above $7x10^{18}$ cm^{-3}. In our preparation procedure, the carrier concentration can be controlled by the additional doping process since there is few Au atom in the prepared GOI layer.

3.4.2 Thermal conductivity analysis

Fig. 3.11 is the thermal conductivity of the Ge layer with and without Au catalyst as a function of annealing temperature. The measured value of the as-deposited Ge layer is 0.82 $Wm^{-1}K^{-1}$, which is close to the reported value[52]. It is found that the crystallized Ge film formed by GIC has larger thermal conductivity than the Ge film formed without Au.

The increase in the thermal conductivity of the MIC-formed Ge film is considered to originate from the crystallization of the Ge film, taking account of the result that the Ge layer contains few Au atoms and the fact that the thermal conductivity in a crystal material is usually larger than that in an amorphous material.

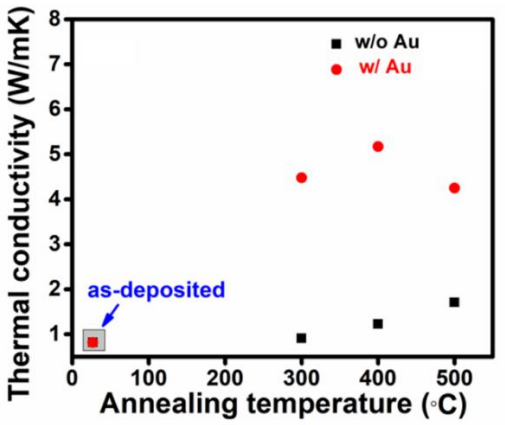

Figure 3.11 Thermal conductivity of Ge film w/o Au and w/ Au catalyst, as a function of annealing temperature.

3.5 Conclusions

Poly-crystalline (pc)-GOI layer w/Au was investigated for a short annealing time and clarified the influence of Au catalyst on the crystallization and the thermoelectric characteristics. After annealing only for 60 min, the pc-GOI layer was successfully obtained by tuning the annealing temperature around the eutectic temperature of the Au-Ge alloy system. The SEM, EPMA, XRD, and Raman scattering spectroscopy results indicate that the Au layer plays a role of enhancing the crystallization and island-formation of the Ge film. As for the thermoelectric characteristics, the Seebeck coefficient is hardly influenced by a small amount of residual Au atoms while the thermal conductivity is increased in the Ge layer, w/Au. This is caused by the crystallinity of the Ge film because the crystallographic properties indicated that there are few Au atoms in the prepared Ge layer.

Chapter 4: Polycrystalline Germanium thin films: Cu induced crystallization of a-Ge

4.1 Background of Cu induced crystallization of a-Ge thin films

Interesting works have been done on Cu induced crystallization of a-Ge[53,54]. The two important properties of metal catalyst Cu in the process of crystallization are the metal catalyst Cu should be effective to enhance the crystallization process at low temperatures and Cu can enhance both the nucleation and the subsequent nucleus growth. Using Cu as a metal catalyst, the crystallized Ge thin film can be achieved with the Ge crystalline particle size in the nanoscale range. Moreover, a thin layer of Ge crystallized thin film can be accomplished. The eutectic temperature of Ge-Cu binary system is 641 ºC[55]. By considering the low-temperature fabrication of polycrystalline Ge using Cu induced crystallization, the annealing condition was employed at 400 ºC for 4 hrs.

The two kinds of annealing process namely, conventional furnace annealing (CFA) and rapid thermal annealing (RTA) were performed at 400 ºC for 4 hrs to check the influences of metal catalyst Cu and the effect of annealing using CFA and RTA, with the starting structure of Cu (20nm)/ Ge (100nm). And the microstructure and thermoelectric characteristics have been investigated with and without the influence of metal catalyst Cu i.e., w/Cu and w/o Cu.

4.2 Experimentation and sample preparation

4.2.1 Sample preparation and growth mechanism

In this study, commercially available SiO_2/Si was pre-cleaned using piranha solution for 1 min. Preparation of Cu and Ge layers on SiO_2(thickness:103nm)/Si(thickness:378µm) substrate was carried out at room temperature. Initially, amorphous-Ge (a-Ge) thin layer (thickness: 100nm) was deposited on

SiO_2/Si substrate, using vacuum evaporation system in a vacuum chamber with a base pressure of 6.0 x 10^{-4} Pa. Consequently, a thin layer of Cu (thickness: 20nm) was deposited on a-Ge/SiO_2/Si substrate, using vacuum evaporation system in a vacuum chamber with a base pressure of 6.0 x 10^{-4} Pa. After that, the sample consists of Cu/a-Ge/SiO_2/Si was subjected to annealing for the Ge crystallization process, at lower eutectic temperature of Cu-Ge binary phase eutectic system of 400º C for 4 hrs, in an N_2 ambient. After the completion of annealing process, the residual Cu metal layer was etched for few seconds. For reference, a-Ge/SiO_2/Si substrate was also annealed at 400º C for 4 hrs, in an N_2 ambient, to check the influence of metal catalyst Cu, during the crystallization process. Ge crystallization process at 400º C for 4 hrs was performed with the conventional furnace annealing (CFA) and rapid thermal annealing (RTA) processes. The experimentation process flow diagram is schematically represented in Figs. 4.1 and 4.3.

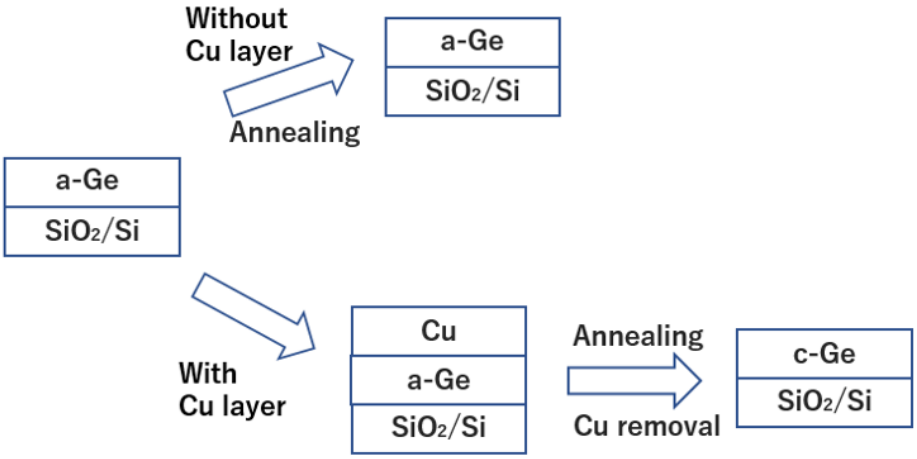

Figure 4.1 Schematic of Cu-induced crystallization process of Ge film on SiO_2/Si substrate, using conventional furnace annealing (CFA) process.

Originally, the as-deposited Ge thin films were in amorphous phase. The Ge crystallization process began with the nucleation process for 30 min, using conventional furnace annealing (CFA) process. During this stage, nuclei were formed with respect to the annealing temperature. Annealing condition was performed below the eutectic temperature of Cu-Ge at 400º C for 4 hrs. The Ge crystals were formed during the crystal growth period of 4 hrs. Fig. 4.2 portrayed the Ge crystal growth mechanism during the

conventional furnace annealing (CFA) process of Cu induced crystallization of a-Ge. No possibility of formation of Cu-Ge alloy, since the annealing process was done below the eutectic temperature of Cu-Ge. After the annealing process, the cooling time was taken for nearly 2 hrs and 30 min and the crystalline phase was achieved.

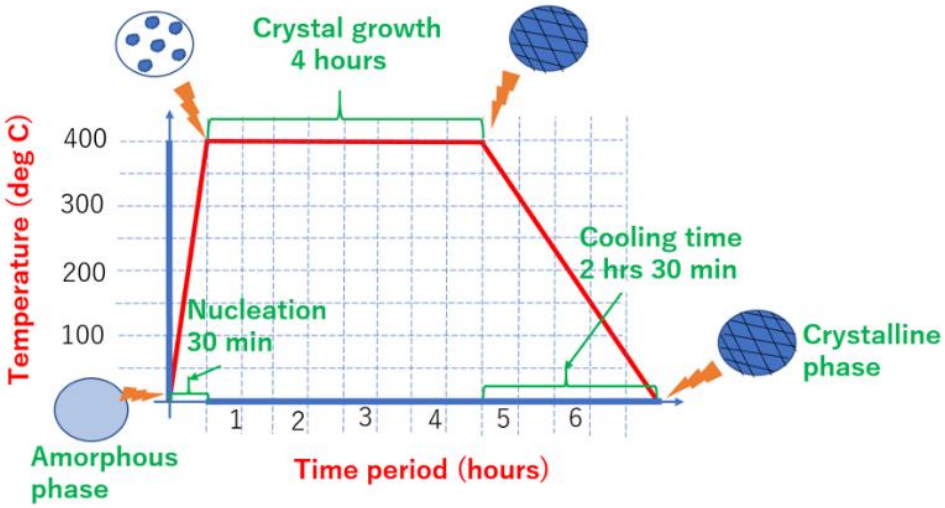

Figure 4.2 Growth mechanism of Cu induced crystallization of Ge, during the conventional furnace annealing (CFA) process.

Firstly, the as-deposited Ge thin films were in amorphous phase. The Ge crystallization process began with the nucleation process for 1 min, using rapid thermal annealing (RTA) process. During this stage, nuclei were formed with respect to the annealing temperature. While comparing with the CFA process, the densification of nuclei was larger, due to sudden rise in temperature of 400º C in 1 min. The same annealing condition was performed to compare the crystallization process of CFA and RTA. As done earlier for CFA process, the annealing condition was done below the eutectic temperature of Ge-Cu at 400º C for 4 hrs. The Ge crystals were formed during the crystal growth period of 4 hrs. Fig. 4.4 described the Ge crystal growth mechanism during the rapid thermal annealing process of Cu induced crystallization of a-Ge. As like as the annealing process by CFA, here also no possibility of formation of Cu-Ge alloy,

since the annealing process was done below the eutectic temperature of Cu-Ge. After the annealing process, the sudden cooling time was taken as 1 min and the crystalline phase was accomplished.

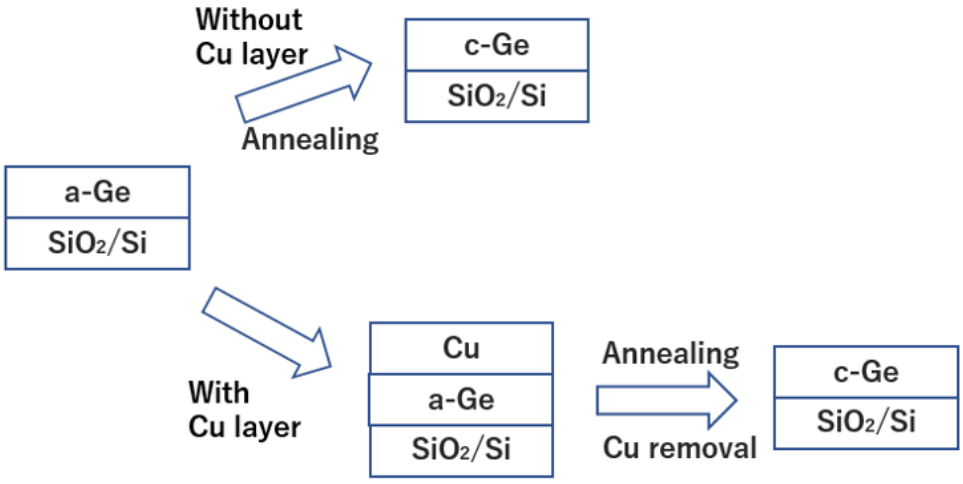

Figure 4.3 Schematic of Cu-induced crystallization process of Ge film on SiO_2/Si substrate, using rapid thermal annealing (RTA) process.

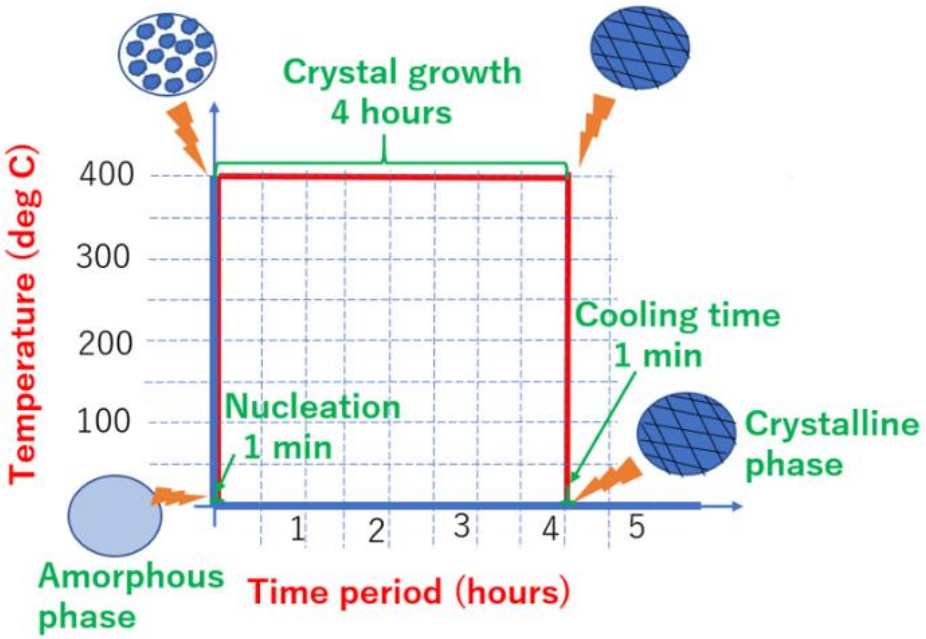

Figure 4.4 Growth mechanism of Cu induced crystallization of Ge, during the rapid

thermal annealing (RTA) process.

4.3 Microstructure Characterization Analysis

4.3.1 Optical microscopy

Fig. 4.5 displays the optical microscopy analysis of the as-deposited and annealed samples, using CFA and RTA processes. Figs. 4.5 (a), (b) show the optical analysis of the as-deposited a-Ge/SiO_2/Si, and Cu/Ge/SiO_2/Si. Figs. 4.5 (c), (d) and (e), (f) exhibit the optical study of the samples annealed at 400º C for 4 hrs, using CFA and RTA processes, for the two cases w/o Cu and w/ Cu. As previously discussed in chapter 3, the changes in the color appearances of the as-deposited samples represented the thin layer depositions on the SiO_2/Si substrate. After annealing at 400º C for 4hrs using CFA, the appearence of the substrate was slightly transformed while comparing with the former. Other than that, no changes were detected for the CFA process, w/o Cu and w/Cu.

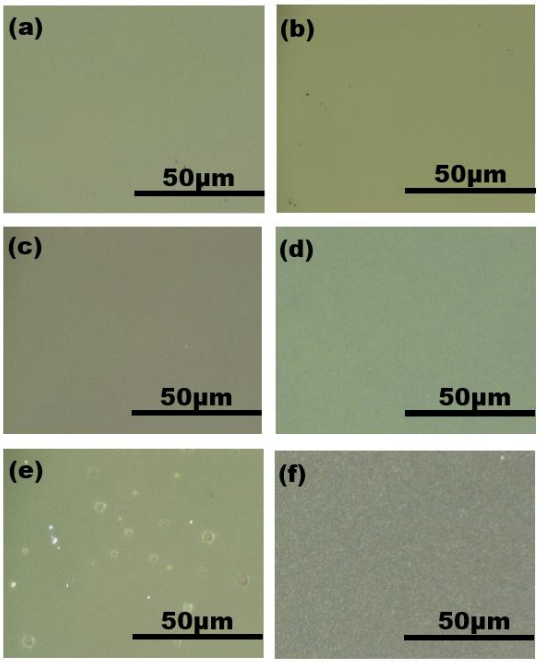

Figure 4.5 Optical microscopy image of the samples over SiO_2/Si at each stage of crystallization

process. (a) a-Ge layer, (b) Cu thin layer. After conventional furnace annealing (CFA) at 400 ºC for 4 hrs, (c) w/o Cu, (d) w/ Cu. After rapid thermal annealing (RTA) at 400 ºC for 4 hrs, (e) w/o Cu, (f) w/ Cu.

For the RTA annealing process at the same temperature, surface modifications were identified with a small number of dots like structure for w/o Cu. The surface discoloration with a large number of a spot like a layer was analyzed for w/Cu, after annealing at 400º C for 4 hrs using RTA.

4.3.2 X-Ray Diffraction (XRD)

XRD profiles of the Ge layers annealed at 400 ºC, 4 hrs for w/o Cu and w/Cu layer using CFA and RTA processes were shown in Figs. 4.6(a) and (b). This result indicates that the Ge layer remains amorphous, w/o Cu using CFA process and in contrast, in the XRD profiles of the Ge layers formed w/Cu using CFA process, (Fig. 4.6 (a)), c-Ge (111) peak at ~27.4º can be clearly observed. Hence, it can be said that the Cu catalyst plays a role in enhancing the crystallization of Ge film, using CFA process.

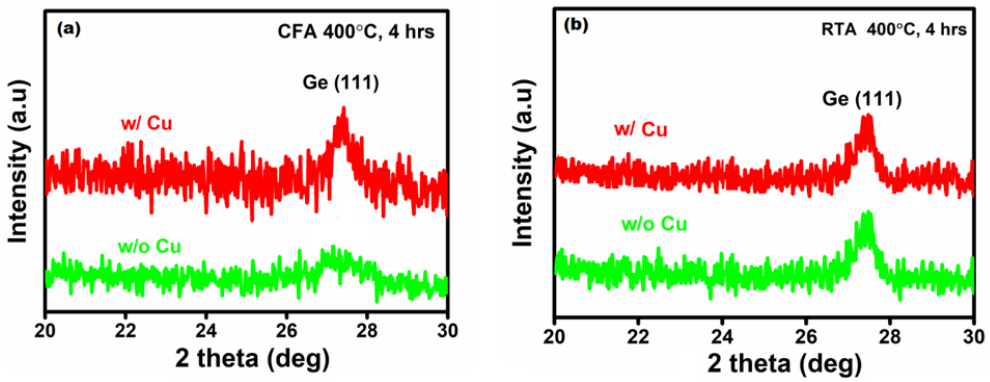

Figure 4.6 XRD profiles of annealed Ge films (a) CFA and (b) RTA.

From Fig. 4.6 (b), the Ge (111) peak becomes more significant even annealing at 400 ºC for 4hrs, w/o Cu using RTA process. While adding the metal catalyst Cu in RTA process, it was identified that the intensity of Ge (111) peak was increased, compared with the w/o Cu, RTA process. RTA process plays a

vital role in the crystallization process, due to its sudden rise in temperature during the nucleation time.

4.3.3 Raman Spectroscopy

Fig. 4.7 (a) and (b) show Raman spectra obtained from the Ge layers annealed at 400 ºC for 4 hrs, w/o Cu and w/Cu layer, using CFA and RTA processes. The a-Ge peak was observed in the prepared Ge layers w/o Cu catalyst even after annealing at 400 ºC for 4 hrs, w/o Cu, using CFA, as shown in Fig. 4.7(a). For the Ge layer, w/ Cu, in contrast, a sharp peak of Ge-Ge bond at 297 cm^{-1} was clearly observed, as shown in Fig. 4.7 (b), which is assigned to c-Ge[48].

From Fig. 4.7 (b), the c-Ge peak becomes more significant even annealing at 400 ºC for 4 hrs, w/o Cu using RTA process. As like as the XRD analysis (Fig. 4.6), the addition of metal catalyst Cu enhances the intensity of c-Ge peaks.

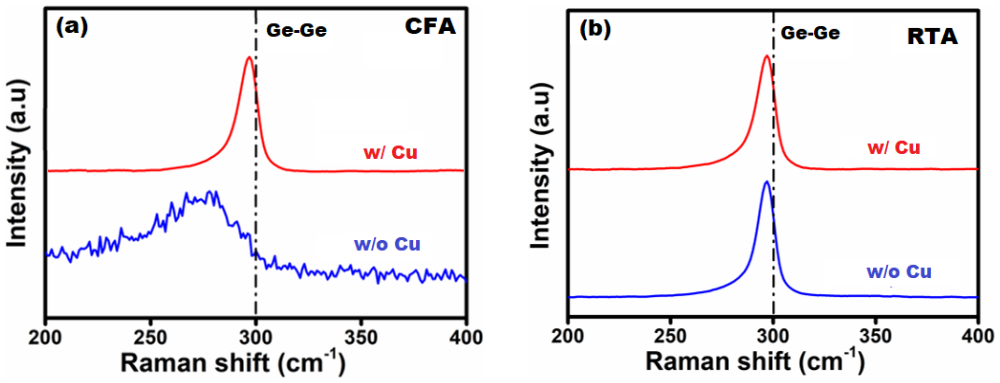

Figure 4.7 Raman spectra of annealed Ge films (a) CFA and (b) RTA.

These findings indicate that the Cu catalyst makes the Ge film crystalized even at 400 ºC for 4 hrs, w/o Cu using RTA process, while the Ge film w/o Cu, using CFA process was dominantly amorphous for the same annealing condition. Raman analysis is consistent with XRD characterization results. The Ge-Ge peak position observed in the Ge film, w/Cu is slightly lower than 300 cm^{-1} in bulk c-Ge, due to amorphous and nano-crystalline Ge present in the layer[49]. Moreover, it was confirmed that Ge-Cu

component is below the detection limit in Raman spectra.

4.3.4 Field Emission-Scanning Electron Microscopy (FE-SEM)

Fig. 4.8 indicates FE-SEM images of the Ge layer surfaces of as-deposited and the samples annealed at 400 ºC for 4hrs, w/o Cu and w/Cu, using CFA and RTA processes. Figs. 4.8 (a) and (b) represent the as-deposited sample surfaces, prior to an annealing process. Uniform thin layer with a large number of smaller Ge-crystals was identified in w/ Cu, while comparing w/o Cu, using CFA, as shown in Figs. 4.8 (c) and (d).

While the Ge layers w/o Cu catalyst seem to have enriched with more uniform smaller grains and for w/ Cu, and the Ge surface identified with some smaller pit-like structure throughout the substrate for the RTA process, as shown in Figs. 4.8 (e) and (f).

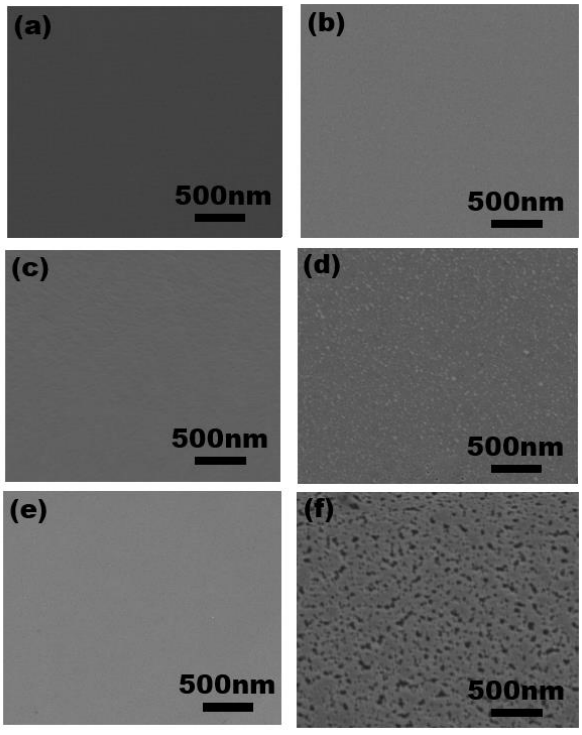

Figure 4.8 FE-SEM images of the Ge layer surfaces (a) as-deposited a-Ge, (b) as-deposited Cu/ a-Ge. After annealing at 400 ºC for 4 hrs, CFA (c) w/o Cu (d) w/ Cu. After annealing at 400 ºC for 4 hrs, RTA (e) w/o Cu (f) w/ Cu.

4.3.5 Field Emission- Electron Probe Micro (FE-EPMA)

Figs. 4.9 and 4.10 represent the EPMA of the samples annealed at 400 ºC for 4 hrs, using CFA and RTA processes. From Fig 4.9 (a), the obtained surface was enriched with more number of smaller grains throughout the substrate with no larger island like structure formation. Ge distribution clearly depicts its presence all over the substrate, as shown in Fig. 4.9 (b). In the elemental line profile, obtained at a yellow line in the EPMA image, Si and O signals were observed, originated from the SiO_2/Si substrate. Also, it clarified the formation of smaller grains which act as a uniform thin layer of Ge surfaces, as represented in Fig. 4.9 (c).

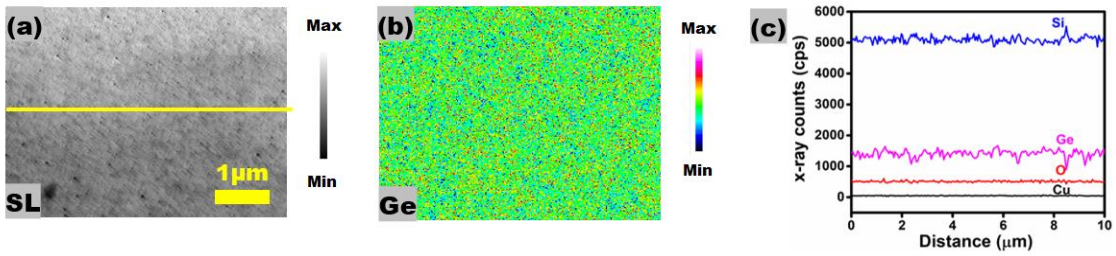

Figure 4.9 After annealing at 400 ºC for 4 hrs, CFA (a) EPMA image, (b) Ge distribution (c) elemental line profile Ge films.

From Fig 4.10 (a), the Ge surface was obtained with smaller grains with small pit-like structure throughout the substrate with the absence of larger grains. Like the CFA process (Fig. 4.9 (b) and (c)), the RTA process of Ge distribution and line profile analysis of EPMA clearly confirm the formation of smaller grains which act as a uniform thin layer of Ge surfaces, as shown in Fig. 4.10 (b) and (c). Also, both CFA and RTA processes were detected with low-level metal contamination in the Ge surfaces. The EPMA is consistent with the obtained FE-SEM characterization results.

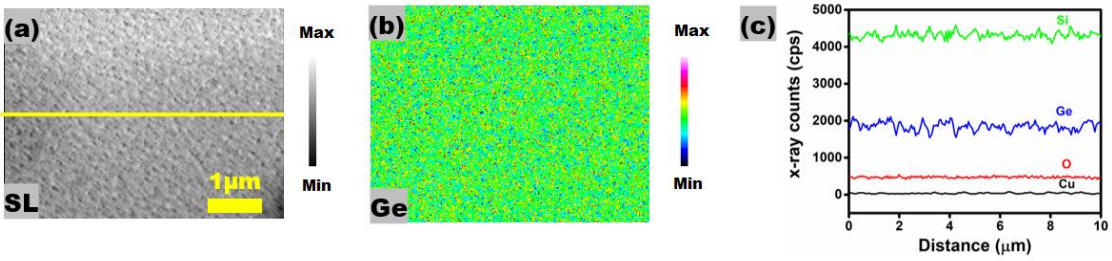

Figure 4.10 After annealing at 400 ºC for 4 hrs, RTA (a) EPMA image, (b) Ge distribution (c) elemental line profile Ge films.

4.3.6 Electron Back Scattering Detector (EBSD)

Fig. 4.11(a) and (b) depict the EBSD images of the samples annealed at 400º C for 4 hrs using CFA and RTA process.

Both the annealed sample showed the poly-crystalline Ge surface with dominant (111)-Ge plane. Since the Ge surfaces were obtained with a uniform thin layer like structure without any larger islands, it was difficult to analyze the grain size. The inset color triangle represents the corresponding orientation of the Ge surfaces. Both the CFA and RTA process clarified the formation of (111)-oriented Ge surfaces and this EBSD analysis is consistent with the XRD and Raman analysis.

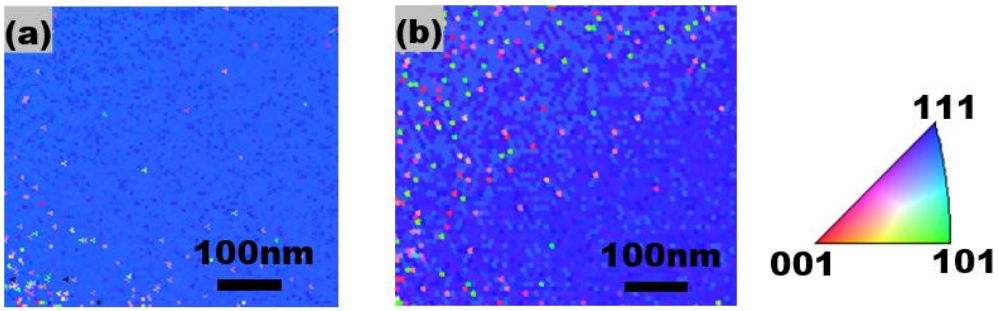

Figure 4.11 EBSD images of the samples annealed at 400º C for 4 hrs, (a) CFA and (b) RTA.

4.3.7 X-ray Photoelectron Spectroscopy (XPS)

Figure 4.12 (a) and (b) exemplify the XPS analysis of the samples annealed at 400º C for 4 hrs

using CFA and RTA, w/o Cu and w/ Cu.

From Fig. 4.12 (a) the samples annealed at 400º C for 4 hrs, using CFA w/o Cu, two peaks were detected at 29.9 and 32.8 eV were assigned to the sub-oxides and oxidation peak of Ge 3d spectra[69-72]. Also, for the samples annealed at 400º C for 4 hrs, using CFA w/ Cu, peak attained at 29.6 eV was assigned to the elemental Ge 3d spectra. From Fig. 4.12 (b), the samples annealed at 400º C for 4 hrs, using RTA w/o Cu, the peak achieved at 30.5 eV was assigned to sub-oxides of elemental Ge 3d spectra. For the same annealing condition using RTA, w/ Cu, the peak achieved at 29.6 eV was assigned to elemental Ge 3d spectra. Hence, the possibility of formation of oxides during the crystallization process is reduced, by utilizing the metal catalyst Cu during the crystallization process.

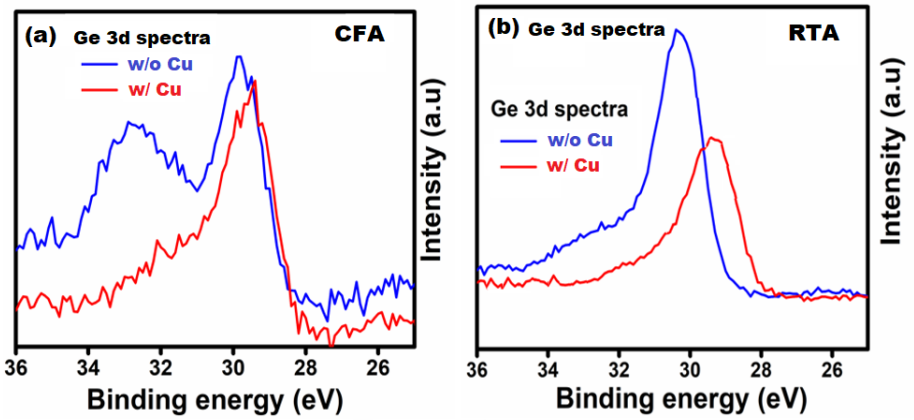

Figure 4.12 XPS analysis of the samples annealed at 400º C for 4 hrs, (a) CFA and (b) RTA.

4.4 Thermoelectric characteristics

4.4.1 Seebeck coefficient measurement

The Seebeck coefficient of the Ge layer using CFA and RTA processes, w/o Cu and w/Cu catalyst were shown in Figs. 4.13(a) and (b), as a function of annealing temperature. The sample condition was represented as X- as deposited a-Ge, Y- 400 ºC, 4 hrs using CFA and Z-400ºC, 4 hrs using RTA processes. The data of the as-deposited Ge layer (X) were also indicated in these graphs for comparison.

The Seebeck coefficient for the Ge layer, w/o Cu and w/ Cu, using CFA and RTA processes could not be measured owing to its high electric resistance, which indicates a small number of carriers in the Ge layer. Although the measured Seebeck coefficients scatter in Figs. 4.13(a) and (b), there was not a significant difference between w/o Cu and w/Cu, using CFA and RTA processes, as previously discussed in Chapter 3.

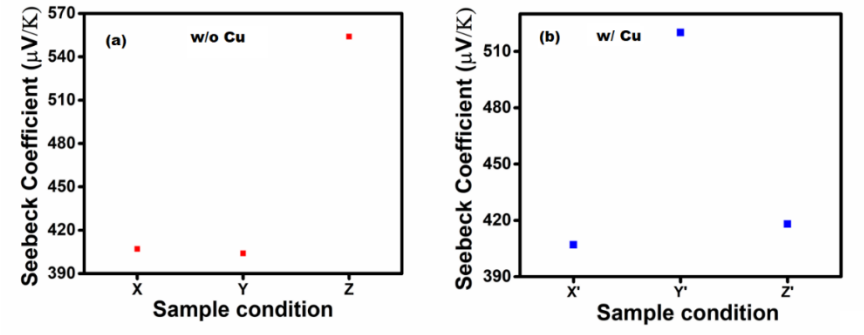

Figure 4.13 Seebeck coefficient of Ge film w/o Cu and w/ Cu, as a function of annealing temperature.

It represented that the metal catalyst Cu could not make Ge-Cu bonds in the Ge thin films and hence the presence of Cu atoms not influenced the seebeck coefficient. Also, the lower level of Cu metal contamination acts as a carrier source and hence the difficulty of controlling the carrier concentration is high.

4.4.2 Thermal conductivity Analysis

Fig. 4.14(a) and (b) are the thermal conductivity of the Ge layers using CFA and RTA processes, w/o Cu and w/ Cu catalyst as a function of annealing temperature. The sample condition was represented as X- as deposited a-Ge, Y- 400 ºC, 4 hrs using CFA and Z-400 ºC, 4 hrs using RTA processes. The measured value of the as-deposited Ge layer is 0.82 $Wm^{-1}K^{-1}$, which is close to the reported value[52].

The attained thermal conductivity value of w/o Cu was close to the as-deposited a-Ge and the higher thermal conductivity value is achieved for w/o Cu, RTA process. Also, it is found that the crystallized Ge film

formed by w/ Cu, RTA process has larger thermal conductivity than the Ge film formed by w/ Cu, CFA and the as-deposited a-Ge. This increase in the thermal conductivity values of CFA and RTA processes, w/o Cu and w/Cu is due to the presence of Cu atoms in low concentration.

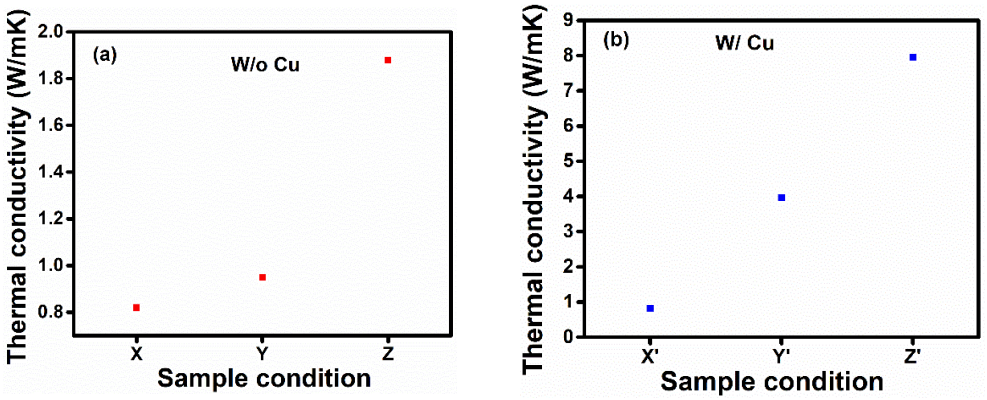

Figure 4.14 Thermal conductivity of Ge film w/o Cu and w/ Cu, as a function of annealing temperature.

4.5 Conclusions

Fabrication of poly-crystalline (pc)-GOI layer was investigated using CFA and RTA process, w/o Cu and w/ Cu at a lower eutectic temperature of 400 ºC for 4hrs and clarified the effective role of RTA process of crystallization. The SEM, EPMA, XRD, and Raman scattering spectroscopy results indicate that the Cu layer plays a role in enhancing the crystallization with the formation of crystallized Ge thin film, using CFA process. Also, the effective Ge crystallization process was clearly demonstrated using RTA process. The presence of a small number of Cu atoms in the crystallized Ge thin film influenced the seebeck coefficient measurement and the larger thermal conductivity value is achieved for the Ge film, w/ Cu, RTA than the as-deposited Ge and w/ Cu, CFA.

Chapter 5: Polycrystalline Germanium thin films: Al induced crystallization of a-Ge

5.1 Background of Al induced crystallization of a-Ge thin films

Al induced crystallization of a-Ge has been investigated in fabricating the poly-crystalline Ge on insulator substrates[58-65]. Peculiarly, Al induced crystallization is gaining interest, because of its low temperature fabrication process. The effective role of using the metal catalyst Al, during the crystallization process is to attain the larger grained poly-crystalline structures with the grain size of 10–100 μm[66]. Moreover, high quality poly-crystalline Ge with larger grain size can also acts as a single Ge crystal substrate[67].

Interestingly, the eutectic temperature of Ge-Al is 421 ^{o}C. By considering the low temperature annealing process, the annealing condition was performed at 350^{o}C for 2 and 4 hrs to fabricate the poly-crystalline Ge, for the starting structure of Al (100nm)/Ge(100nm), using rapid thermal annealing (RTA) process. And the microstructure and thermoelectric characteristics has been investigated with and without the influence of metal catalyst Al i.e., w/ Al and w/o Al.

5.2 Experimentation and sample preparation

5.2.1 Sample preparation and growth mechanism

In this study, commercially available SiO_2/Si was pre-cleaned using piranha solution for 1 min. Preparation of Al and Ge layers on SiO_2(thickness:103nm)/Si(thickness:378μm) substrate was carried out at room temperature. Initially, amorphous-Ge (a-Ge) thin layer (thickness: 100nm) was deposited on SiO_2/Si substrate, using vacuum evaporation system in a vacuum chamber with a base pressure of 6.0 x 10^{-4} Pa. Consequently, a thin layer of Al (thickness: 100nm) was deposited on a-Ge/SiO_2/Si substrate, using

vacuum evaporation system in a vacuum chamber with a base pressure of 6.0 x 10^{-4} Pa. After that, the sample consists of Al/a-Ge/SiO_2/Si was subjected to rapid thermal furnace annealing for the Ge crystallization process, at lower eutectic temperature of 350º C for 2 and 4 hrs, in an N_2 ambient. After the completion of rapid thermal furnace annealing (RTA) process, the residual Al metal layer was etched using HF solution for few seconds. For reference, a-Ge/SiO_2/Si substrate was also annealed at 350º C for 2 and 4hrs, in an N_2 ambient, to check the influence of metal catalyst Al, during the crystallization process. The experimentation process flow diagram is schematically represented in Fig. 5.1.

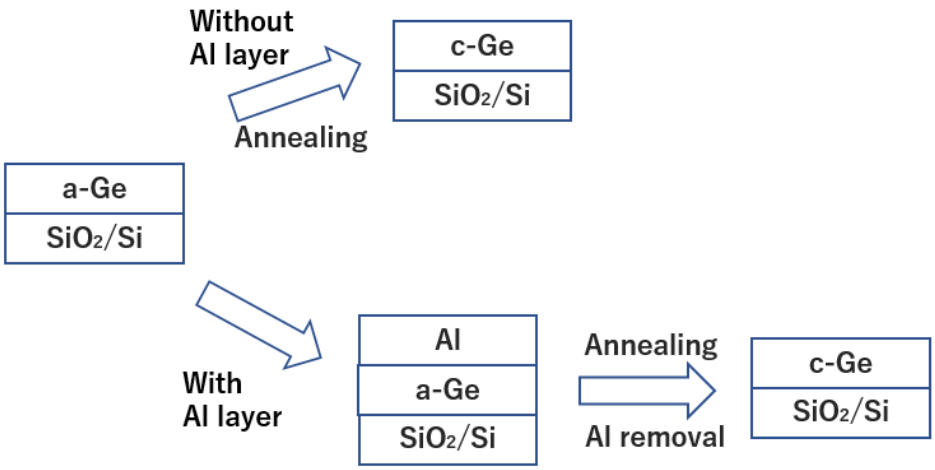

Figure 5.1 Schematic of Al-induced crystallization process of Ge film on SiO_2/Si substrate, using rapid thermal annealing (RTA) process.

Primarily, the as-deposited Ge thin films were in amorphous phase. The Ge crystallization process began with the nucleation process for 1 min, using rapid thermal annealing (RTA) process. During this stage, nuclei were formed with respect to the annealing temperature of 350º C in 1 min, as nucleation time. As done earlier in chapter 4, the annealing condition was chosen below the eutectic temperature of Ge-Al[68]. The Ge crystals were formed during the crystal growth period of 2 hrs at 350º C. Fig. 5.2 represents the Ge crystal growth mechanism during the rapid thermal annealing process of Al induced crystallization

of a-Ge. After the annealing process, the sudden cooling was performed for 1 min and the crystalline phase was accomplished.

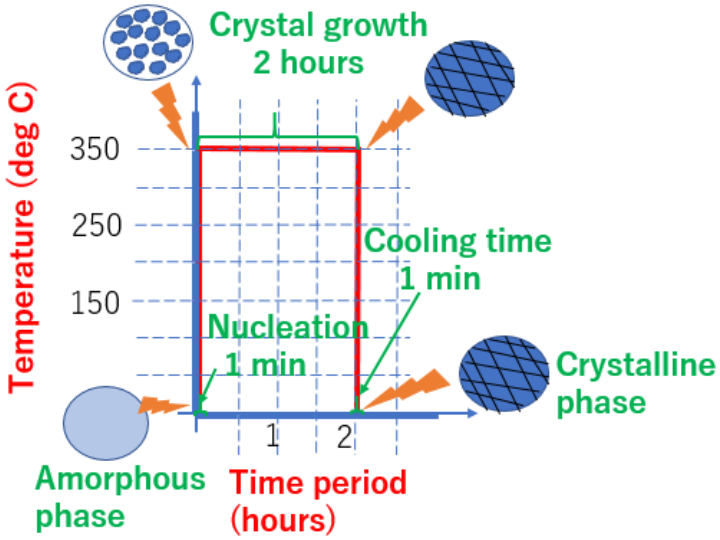

Figure 5.2 Growth mechanism of Al induced crystallization of Ge, during rapid thermal annealing (RTA) process at 350 °C for 2 hrs.

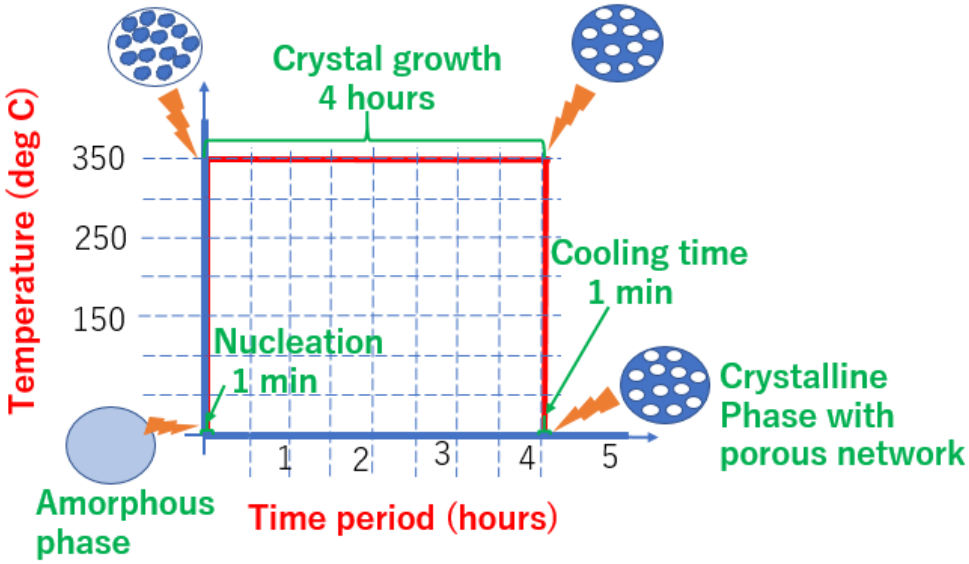

Figure 5.3 Growth mechanism of Al induced crystallization of Ge, during rapid thermal

annealing (RTA) process at 350 ºC for 4 hrs.

The same crystallization steps were repeated starting from the amorphous phase with nucleation time of 1 min, using RTA process. As done earlier, nuclei were formed during the nucleation phase. Here, the annealing operation was performed at 350º C for 4 hrs. The Ge crystals with porous networks were formed during the crystal growth period of 4 hrs. Fig. 5.3 represents the Ge crystal growth mechanism during the rapid thermal annealing process of Al induced crystallization of a-Ge. After the annealing process, the sudden cooling was performed for 1 min and the crystalline phase with porous network was attained. During the above RTA processes of Al induced crystallization of a-Ge, no possibility of formation of Al-Ge alloy, since the annealing process was performed below the eutectic temperature of Al-Ge.

5.3 Microstructure Characterization Analysis

5.3.1 Optical microscopy

Fig. 5.4 presents the optical microscopy analysis of the as-deposited and annealed samples, using RTA of Al induced crystallization of a-Ge. Figs.5.4 (a) and (b) show the optical analysis of the as-deposited a-Ge/SiO_2/Si, and Al/Ge/SiO_2/Si. Figs.5.4 (c)-(d) and (e)-(f) exhibit the optical study of the samples annealed at 350º C for 2 and 4 hrs, for the two cases, w/o Al and w/ Al. As previously discussed in chapters 3 and 4, the changes in the color appearances of the as-deposited samples represented the thin layer depositions on the SiO_2/Si substrate. After annealing at 350º C for 2 and 4hrs, the appearance of the Ge layers, w/ Al was drastically changed while comparing with the Ge layers, w/ Al. For 2 hrs annealing condition, larger grain like structure was observed, whereas in 4 hrs annealing condition, crystalline grains with some spaces in between were observed.

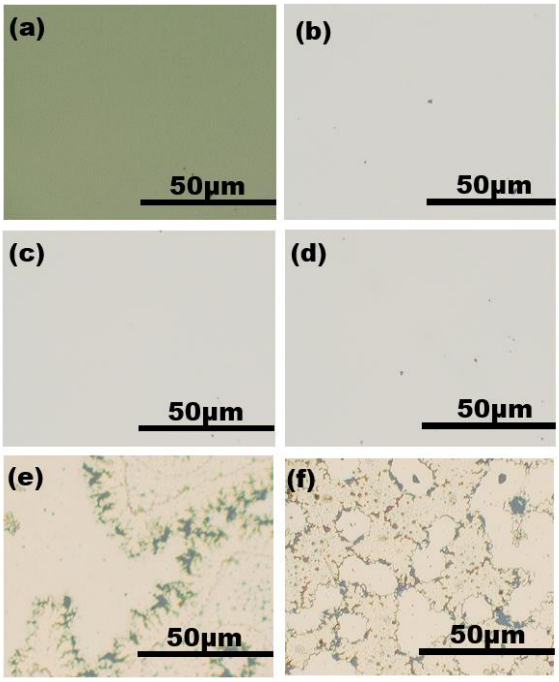

Figure 5.4 Optical microscopy image of the samples over SiO_2/Si at each stage of crystallization process. (a) a-Ge layer, (b) Al thin layer. After rapid thermal annealing (RTA) at 350 ºC for 2 hrs, (c) w/o Al, (d) w/ Al. After rapid thermal annealing (RTA) at 350 ºC for 4 hrs, (e) w/o Al, (f) w/ Al.

5.3.2 X-Ray Diffraction (XRD)

XRD profiles of the Ge layers annealed at 350 ºC, 2 and 4 hrs for w/o Al and w/ Al layer, using RTA process were shown in Figs. 5.5 (a) and (b). This result indicates that the as deposited a-Ge layer started to crystallize even after annealing at 350 ºC for 2 hrs, w/o Al as shown in Fig.5.5(a). A low intensity c-Ge (111) peak at ~27.4º was observed. On increasing the annealing time for 4 hrs at 350 ºC, w/o Al the intensity of the c-Ge peak was further increased. From Fig. 5.5 (b), after annealing at 350 ºC for 2 and 4 hrs, w/ Al the intensity of the c-Ge peak was increased further. Hence, it can be said that the Al catalyst plays a role of enhancing the crystallization of Ge film, using RTA process.

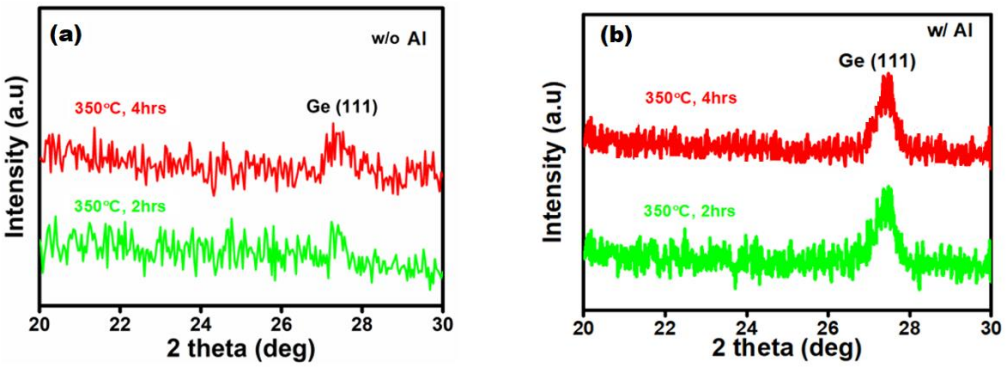

Figure 5.5 XRD profiles of annealed Ge films (a) w/o Al and (b) w/ Al.

5.3.3 Raman Spectroscopy

Figs. 5.6 (a) and (b) show Raman spectra obtained from the Ge layers annealed at 350 ºC for 2 and 4 hrs, w/o Al and w/ Al layer, using RTA process. For the Ge layer, annealing at 350 ºC for 2 and 4 hrs, w/o Al, Raman peaks were identified at 297 cm^{-1}, as represented in Fig. 5.6 (a). For the Ge layer, annealing at 350 ºC for 2 and 4 hrs, w/ Al, sharp peaks of Ge-Ge bond at 299 cm^{-1} were clearly observed, as shown in Fig. 5.6 (b), which is assigned to c-Ge[48].

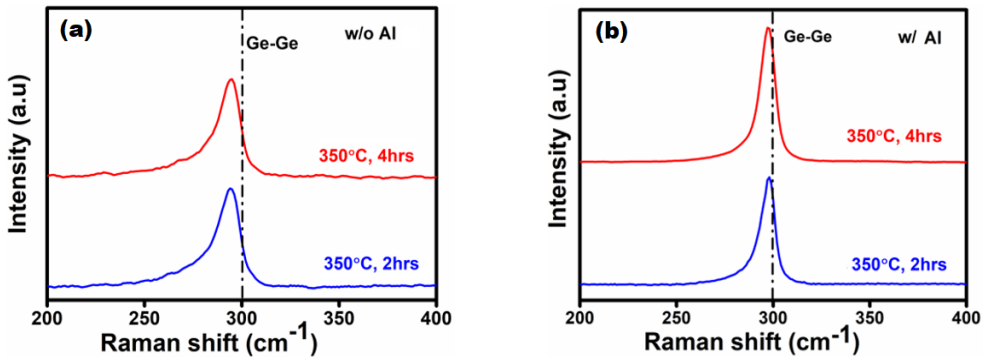

Figure 5.6 Raman spectra of annealed Ge films (a) w/o Al and (b) w/ Al.

These findings indicate that the Al catalyst makes the Ge film partially crystallized even at 350 ºC for 2 and 4 hrs, w/o Al using RTA process, while the Ge film w/ Al, for the same annealing condition dominant c-Ge peaks close to Ge-Ge vibrational bond were observed. Raman analysis is consistent with

XRD characterization results. The Ge-Ge peak position observed in the Ge film, w/ Al is almost 300 cm^{-1}, and this confirms the formation of nano-crystalline Ge present in the layer[49]. Moreover, it was confirmed that Ge-Al component is below the detection limit in Raman spectra.

5.3.4 Field Emission-Scanning Electron Microscopy (FE-SEM)

Fig. 5.7 indicates FE-SEM images of the Ge layer surfaces of as-deposited and the samples annealed at 350 ºC for 2 and 4 hrs, w/o Al and w/ Al, using RTA process. Figs. 5.7 (a) and (b) signify the as-deposited sample surfaces of a-Ge and Al/a-Ge. A minor change were observed after annealing the Ge at 350 ºC for 2 and 4 hrs, w/o Al, as shown in Figs. 5.7 (c) and (d).

From Fig. 5.7 (e), it can be clearly seen that larger Ge islands were formed after annealing at 350 ºC for 2 hrs, w/ Al. On further increasing the annealing time of 4 hrs at 350 ºC, the Ge islands were interconnected together at some edges and later formed as a crystalline porous network as represented in Fig. 5.7 (f).

5.3.5 Field Emission- Electron Probe Micro (FE-EPMA)

Figs. 5.8 and 5.9 represent the EPMA of the samples annealed at 350 ºC for 2 and 4 hrs, using RTA process. From Fig. 5.8(a), it was clearly seen that larger Ge islands were formed after annealing at 350 ºC for 2 hrs, using RTA process. Ge distribution and line profile analysis clearly depicts the larger Ge island over the substrate as shown in Figs. 5.8 (b) and (c). In the elemental line profile, obtained at a yellow line in the EPMA image clarified the position of Ge island over the substrate, in addition Si and O signals were observed, due to the SiO_2 substrate, as represented in Fig. 5.8 (c).

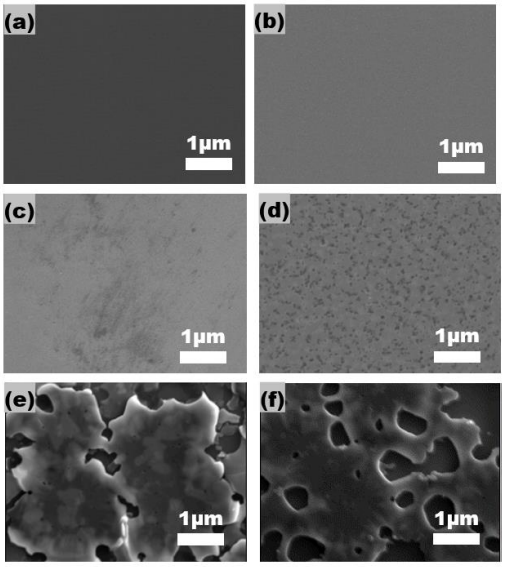

Figure 5.7 FE-SEM images of the Ge layer surfaces (a) as-deposited a-Ge, (b) as-deposited Al/ a-Ge. After annealing at 350 ºC for 2 hrs, RTA (c) w/o Al (e) w/ Al. After annealing at 350 ºC for 4 hrs, RTA (d) w/o Al (f) w/ Al.

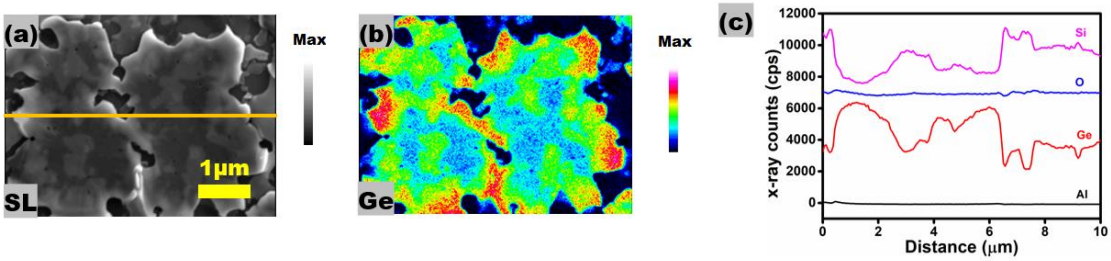

Figure 5.8 After annealing at 350 ºC for 2 hrs, RTA (a) EPMA image, (b) Ge distribution (c) elemental line profile Ge films.

From the EPMA image of Fig 5.9(a), the Ge surface was obtained with the interconnected Ge islands - porous network like structure throughout the substrate. Ge distribution and line profile analysis of EPMA clearly confirm the formation of Ge islands with porous network. From Figs. 5.9 (b) and (c), Ge distribution ang line profile analysis confirm the presence of Ge island with porous network over the substrate. The EPMA is consistent with the obtained FE-SEM characterization results.

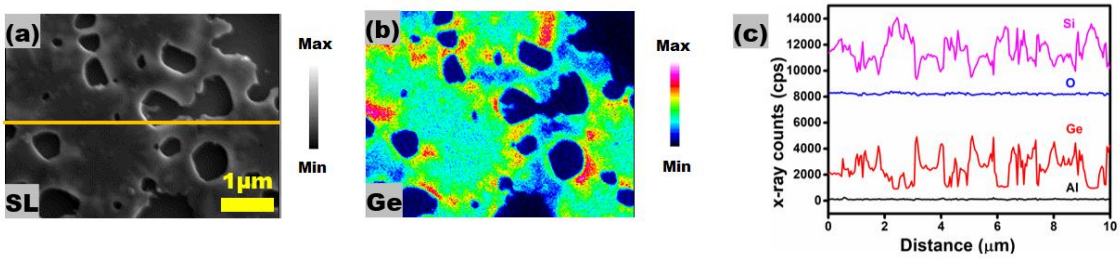

Figure 5.9 After annealing at 350 ºC for 4 hrs, RTA (a) EPMA image, (b) Ge distribution (c) elemental line profile Ge films.

5.3.6 Electron Back Scattering Detector (EBSD)

Fig. 5.10 (a) and (b) portray the EBSD images of the samples annealed at 350º C for 2 and 4 hrs, w/Al. Both the annealed sample shown the poly-crystalline Ge surface with mixed orientation of (111), (101) and (001). The inset color triangle represents the corresponding orientation of the Ge surfaces. EBSD analysis is in good agreement with the obtained FESEM characterization result. The average calculated grain size is about 1-2μm.

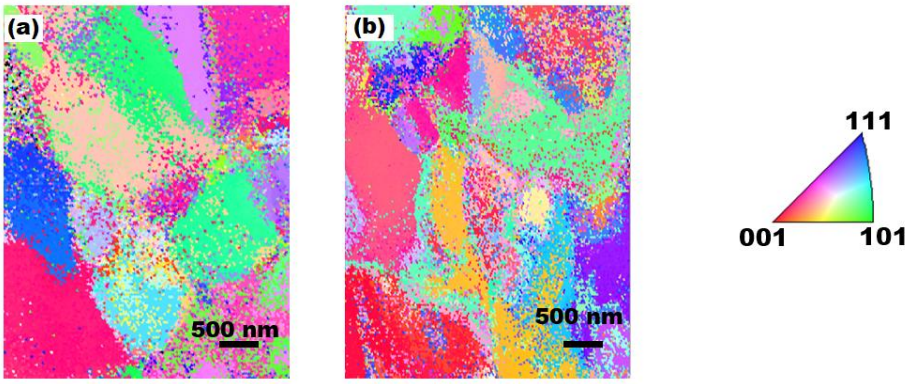

Figure 5.10 EBSD images of the samples annealed at 350º C (a) 2 hrs and (b) 4 hrs.

5.3.7 X-ray Photoelectron Spectroscopy (XPS)

Figure 5.11(a) and (b) represents the XPS analysis of the samples annealed at 350º C for 2 and 4 hrs, w/o Al and w/ Al. From Fig. 5.11 (a) w/o Al, for the sample annealed at 350º C for 2 and 4 hrs, the

peaks obtained at 30.4 and 30.3 eV were assigned to sub-oxides of Ge 3d elemental spectra[69-72]. In contrast, for the sample annealed at 350º C for 2 and 4 hrs, w/Al, the peaks attained at 29.4 and 29.6 eV, corresponded to the elemental Ge 3d spectra, as shown in Fig. 5.11(b). This small shift is likely due to the interaction of interfacial oxide layer during the crystallization, w/o Al. Hence, it is necessary to use the metal catalyst Al, to avoid the oxidation during the crystallization process.

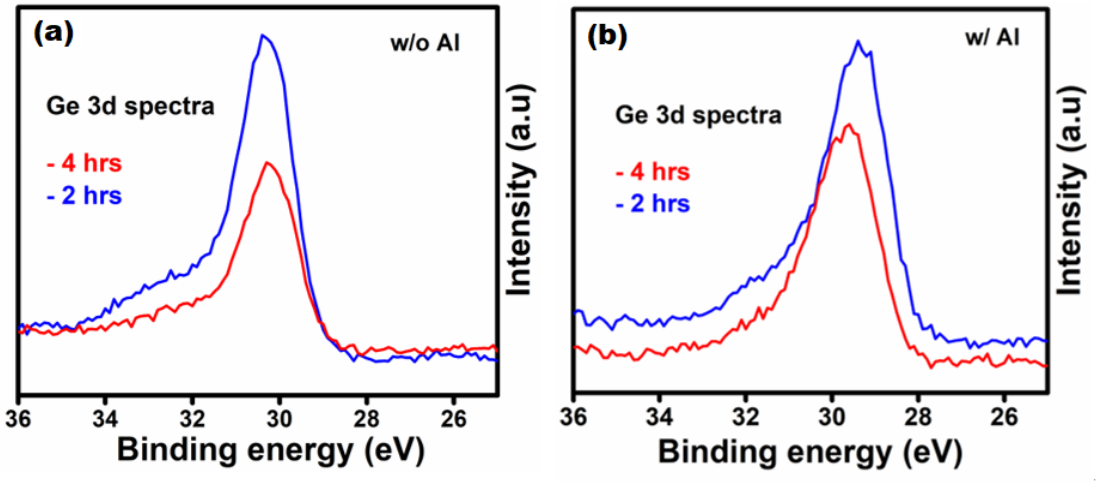

Figure 5.11 XPS analysis of the samples annealed at 350º C for 2 and 4 hrs, (a) w/o Al and (b) w/ Al.

5.4 Thermoelectric characteristics

5.4.1 Seebeck coefficient measurement

The Seebeck coefficient of the Ge layer w/o Al and w/ Al catalyst were shown in Fig. 5.12, as a function of annealing time interval. The measured Seebeck coefficients scatter in Fig. 5.12, hence there is not significant difference between w/o Al and w/ Al after annealing at 350 ºC for 2 and 4 hrs.

As previously discussed in Chapters 3 and 4, it is reported that Al atoms remain in the Ge layer and can acts as a carrier source in Al/Ge bilayers thin film. Hence, the seebeck coefficient is not influenced much. Also, it is not confirmed that Ge and Al are bonded in the Ge film. Some low-level metal

contaminants present in the crystallized Ge thin film makes the scattering value of seebeck coefficient. Hence, the carrier concentration could be controlled by further doping the Ge film, in which low level Al atoms already present.

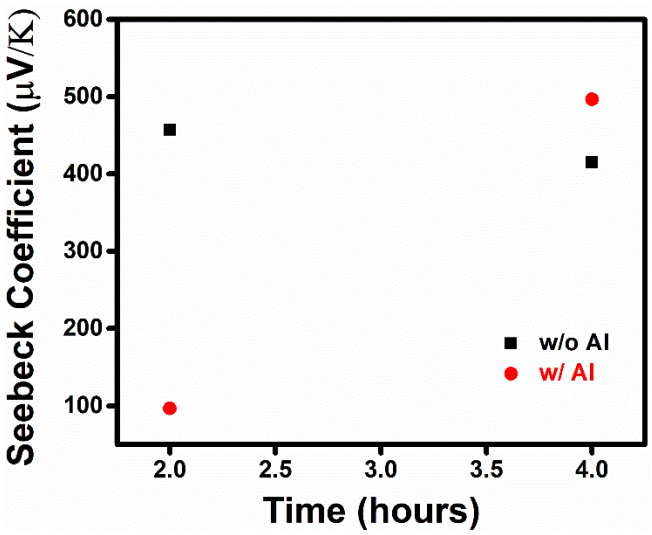

Figure 5.12 Seebeck coefficient of Ge film w/o Al and w/ Al, as a function of annealing temperature.

5.4.2 Thermal conductivity analysis

Fig. 5.13 is the thermal conductivity of the Ge layer, w/o Al and w/ Al catalyst as a function of annealing time interval. A seen from previous chapters 3 and 4, the measured value of the as-deposited Ge layer is 0.82 $Wm^{-1}K^{-1}$, which is close to the reported value.

The attained thermal conductivity value of w/o Al for 2 hrs was close to the as-deposited a-Ge and for the case of w/o Al for 4hrs, the thermal conductivity value was lower than the as-deposited a-Ge. Also, it is found that the crystallized Ge film formed by w/ Al for 4 hrs has larger thermal conductivity than the Ge film formed by w/o Al for 2 hrs, during the RTA process. Presence of lower concentration of Cu atoms in the crystallized Ge increases the thermal conductivity values, during the RTA process.

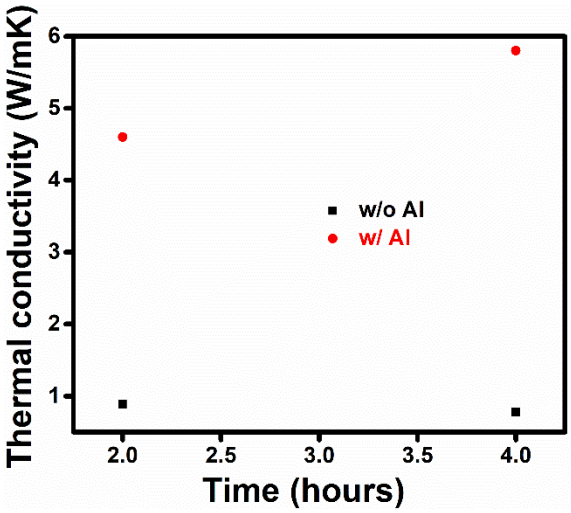

Figure 5.13 Thermal conductivity of Ge film w/o Al and w/ Al, as a function of annealing time period.

5.5 Conclusions

Fabrication of poly-crystalline Ge and its thermoelectric characteristics were investigated at an annealing temperature of 350 ºC for 2 and 4 hrs, w/o Al and w/ Al using RTA process. The SEM, EPMA, XRD, and Raman scattering spectroscopy results indicate that the Al layer plays a role of enhancing the crystallization with Ge larger island-formation and interconnected porous network, after annealing at lower eutectic temperature of Ge-Al of about 2 and 4 hrs. As like the previous chapters 3 and 4, the presence of smaller residual Al atoms hardly influences the thermoelectric characteristics of crystallized Ge thin films on insulators.

Chapter 6: Conclusions

6.1 Conclusions and Future directions

The major results of this thesis are summarized here.

Chapter 2 gives the investigation of thermoelectric and crystallographic studies on Au induced crystallization of a-Ge. The crystallization process was performed around the eutectic temperature of Ge-Au mixture at 300 ºC, 400 ºC and 500 ºC for 60 min, for the starting structure of metal catalyst Au (20nm)/a-Ge (100nm), using the conventional furnace annealing process. The microstructure characterization reveals the crystallographic analysis of poly-crystalline Ge on insulators. The SEM, EPMA, XRD, and Raman scattering spectroscopy results indicate that the Au layer plays a role of enhancing the crystallization and island-formation of the Ge film. As for the thermoelectric characteristics, the seebeck coefficient is hardly influenced by a small amount of residual Au atoms while the thermal conductivity is increased in the Ge layer, w/Au. This is caused by the crystallinity of the Ge film because the crystallographic properties indicated that there are few Au atoms in the prepared Ge layer.

Chapter 3 extends the work of investigation of thermoelectric and crystallographic studies from Au induced crystallization to Cu induced crystallization of a-Ge. The crystallization process was performed at 400 ºC for 4 hours, which is lower than the eutectic mixture of Ge-Cu. The annealing process of conventional furnace and rapid thermal were discussed for the starting structure of metal catalyst Cu (20nm)/a-Ge (100nm). The SEM, EPMA, XRD, and Raman scattering spectroscopy results indicate that the Cu layer plays a role in enhancing the crystallization with the formation of crystallized Ge thin film, using CFA process. Also, the effective Ge crystallization process was clearly demonstrated using RTA process. The presence of a small number of Cu atoms in the crystallized Ge thin film influenced the seebeck coefficient measurement and the larger thermal conductivity value is achieved for the Ge film, w/ Cu, RTA than the as-deposited Ge and w/ Cu, CFA.

Chapter 4 further extends the work on investigation of thermoelectric and crystallographic studies from Cu induced crystallization to Al induced crystallization of a-Ge. The crystallization process was performed at 350 ºC for 2 and 4 hours, which is lower than the eutectic mixture of Ge-Al, using rapid thermal annealing process for the starting structure of metal catalyst Al (100nm)/a-Ge (100nm). The SEM, EPMA, XRD, and Raman scattering spectroscopy results indicate that the Al layer plays a role of enhancing the crystallization with Ge larger island-formation and interconnected porous network, after annealing at lower eutectic temperature of Ge-Al of about 2 and 4 hrs. As like the previous chapters 3 and 4, the presence of smaller residual Al atoms hardly influences the thermoelectric characteristics of crystallized Ge thin films on insulators.

By understanding the above results, the investigation on thermoelectric and crystallographic studies of poly-crystalline Ge pays can be proposed to future directions. From, the above facts, poly-crystalline Ge was formed during the metal induced crystallization of a-Ge, with the influence of catalytic metals like Au, Cu and Al. The obtained characterization results are in good agreement with the other characterization results. By extending the work, with the additional doping process, it can be believed that the seebeck coeffiecient of the crystalline Ge film will be increased, so that the thermoelectric efficiency will also be increased.

List of publications

Journal publications

1. S. Shanthi, K. Faizan, S. Nishino, M. Omprakash, T. Takeuchi, Y. Shimura,Y. Hayakawa, C. Muthamizhchelvan, and H. Ikeda, "Influence of Au on Ge crystallization and its thermoelectric properties in a Au-induced Ge crystallization technique" Journal of Advances in Physics, 2018, 14, 5460-5466.

Conference presentations

1. Masaya Wanami, Selvaraj Shanthi, Yuya Ota, Yehei Suzuki, Faiz Salleh, Masaru Shimomura,
Kenji Murakami, Hiroya Ikeda, "Thermal Studies of ZnO nanostructures on Eco-friendly
Cotton Fabrics for Flexible Thermoelectric Generators", Inter Academia-2016, Warsaw, Poland.

2. Selvaraj Shanthi, Masaya Wanami, Yuya Ota, Faiz Salleh, Yosuke Shimura, Yasuhiro Hayakawa, Hiroya Ikeda, "Structural Analysis of Au-Induced Crystallization of Amorphous Ge for IR Photodetector Applications", Takayanagi Kenjiro Memorial Symposium, Shizuoka University, Hamamatsu, November 2016.

3. Selvaraj Shanthi, Yosuke Shimura, Faiz Salleh, Suru Ponnusamy, Chellamuthu Muthamizhchelvan, Yasuhiro Hayakawa, Hiroya Ikeda, "Low temperature preparation of pc-Ge on SiO_2/Si Substrate by Au induced crystallization", The 10th International Conference on Silicon Epitaxy and heterostructures (ICSI-10), 14 - 19th May 2017 The University of Warwick, Coventry, UK.

4. Selvaraj Shanthi, Yosuke Shimura, Faiz Salleh, Suru Ponnusamy, Chellamuthu Muthamizhchelvan, Yasuhiro Hayakawa, Hiroya Ikeda, "Enhanced Metal Induced Lateral Solid Phase crystallization of Ge on SiO_2/Si Substrate with Au melting-induced Seeding", Takayanagi Kenjiro Memorial Symposium, Shizuoka University, Hamamatsu, November 2017.

References

(1) Landman, U.; Barnett, R. N.; Scherbakov, A. G.; Avouris, P. Phys. Rev. Lett. 2000, 85, 1958.

(2) Zhang, Y. F.; Tang, Y. H.; Wang, N.; Lee, C. S.; Bello, I.; Lee, S. T. Phys. Rev. *B* 2000, 61, 4518.

(3) Lu, X. M.; Ziegler, K. J.; Ghezelbash, A.; Johnston, K. P.; Korgel, B. A. Nano Lett. 2004, 4, 969.

(4) Li, Q.; Chen, C.; Chen. Z.;Jiao, Z.; Wu, M.; Shek, C.H.; Wu, C.M.L.; Lai, J.K.L.;Inorg. Chem., 2012, 51, 8473.

(5) Jung, S M.; Kang, H L.; Won, J K.; Kim, J H.; Hwang, C H.; Ahn, K H.; Chung, I.; Ju. B K.; Kim, M G.; Park, S K. ACS Appl. Mater. Inter. 2018, 10, 3739.

(6) Kima, Y.; Kima, K.; Kim, C Z.; Jung, S H.; Kang, H K.; Park, W K.; Lee, J. Solar Energy Materials & Solar Cells 2017, 166, 127.

(7) Lim, L Y.; Liu, N.; Cui, Y.; Toney, M F. Chem. Mater. 2014, 26, 3739.

(8) Toko, K.;Yoshimine, R.;Moto, K.;Suemasu, T. Scientific reports, 2017, 7, 1.

(9) Takeuchi, W.; Taoka, N.; Kurosawa, M.; Sakashita, M.; Nakatsuka, O.; Zaima, S. Appl. Phys. Lett. 2015, 107, 02210.

(10) Sadoh, T.; Kai, Y.; Matsumura, R.; Moto, K.; Miyao, M. Appl. Phys. Lett. 2016, 109, 232106.

(11) Wang, D.; Chang, Y L.; Wang, Q.; Cao, J.; Farmer, D B.; Gordon, R G.; Dai, H. J. Am. Chem. Soc. 2004, 126, 11602.

(12) Takeuchi, W.; Taoka, N.;, Kurosawa, M.; Sakashita, M.; Nakatsuka, O.; Zaima, S.; Appl. Phys. Lett. 2015, 107, 022103.

(13) Huang, W H.; Shieh, J M.; Kao, M H.; Shen, C H.; Huang, T E.; Wang, H H.; Yang, C C.; Hsieh, T Y.; Hsieh, J L.; Yu, P.; Yeh, W K. Appl. Phys. Exp. 2017, 10, 026502.

(14) Yang, M J.; Shieh, J.; Hsu, S L.; Huang, I J.; Leu, C C.; Shen, S W.; Huang, T Y.; Lehnen, P.; Chien, C

H. Electrochem. Solid-State Lett. 2005, 8, C74.

(15) Toko, K.; Nakao, I.; Sadoh, T.; Noguchi, T.; Miyao, M. Sol. Stat. Electron. 2009, 53, 1159.

(16) Hu, S.; Marshall, A F.; and Mc Intyre, P C. Appl. Phys. Lett. 2010, 97, 082104.

(17) Park, J H.; Kapur, P.; Saraswat, K. C.; Peng, H. Appl. Phys. Lett. 2007, 91,143107.

(18) Wang, Z. M.; Wang, J.; Jeurgens, L.; Mittemeijer, E. 2006, Scr. Mater. 55, 987.

(19) Tan, Z.; Heald, S.; Rapposch, M.; Bouldin, C.; Woicik, J. Phys. Rev. B. 1992, 46, 9505.

(20) Konno, T. J.; Sinclair, R. Philos. Mag. 1995, B 71, 179.

(21) Hekmatshoar, B.; Mohajerzadeh, S.; Shahrjerdi, D.; Robertson, M. D. Appl. Phys. Lett. 2004, 85, 1054.

(22) Herd, S. R.; Chaudhari, P.; Brodsky, M. H. J. Non-Cryst. Sol. 1972, 7, 309.

(23) Zanatta, R.; Chambouleyron, I. J. Appl. Phys. 2005, 97, 094914.

(24) Kanno, H.; Aoki, T.; Atsushi Kenjo, K.; Sadoh,T.; Miyao, M. Mater. Sci. in Semi. Pro. 2005, 8, 79.

(25) Aoki,T.; Kanno, H.; Kenjo, A.; Sadoh, T.; Miyao, M. Thin Solid Films 2006, 508, 44.

(26) Toko, K.; Nakazawa, K.; Saitoh, N.; Yoshizawa, N.; Suemasu, T. Cryst. Grow. Des. 2015, 15, 1535.

(27) Nast, O.; Puzzer, T.; Koschier, L. M.; Sproul, A.B.; Wenham. S.R. Appl. Phys. Lett. 1998, 73, 3214.

(28) Nast, O.; Hartmann, A. J. J. Appl. Phys.2000, 88, 716.

(29) Kurosawa, M.; Tsumura, Y.; Sadoh, T.; Miyao, M. Jpn. J. Appl. Phys. 2009, 48, 03B002.

(30) Wan,Z.; Huang,S.; Green, M.A.; Conibeer, G.; Nanoscale Research Letters 2011, 6,129.

(31) Powell, CF; Oxley, J.H; Blocher Jr, JM *Vapor Deposition*; Wiley, New York, 1967.

(32) Mattox, DM *Handbook of Physical Vapor Deposition (PVD) Processing: Film Formation, Adhesion, Surface Preparation and Contamination Control*; New York, 2004.

(33) Plawsky, J.L.; Fedorov, A. G.; Garimella , S. V.; Ma, H. B.; Maroo , S. C.; Chen, L.; Nam, Y.; Nanoscale and Microscale Thermophysical Engineering,2014, 18, 251.

(34) Salleh, F.; Asai, K.; Ishida, A.; Ikeda, H.; Appl. Phys. Exp. 2009, 2, 071203.

(35) Ikeda, H.; and Salleh, F.; Appl. Phys. Lett. 2010, 96, 012106.

(36) Baba, T.; Jpn. J. Appl. Phys.2009, 48, 05EC01.

(37) Okamoto, Y.; Saeki, J.; Ohtsuki, T.; and Takiguchi, H. Appl. Phys. Exp. 2008, 1, 1170011.

(38) Aono, M.; Ueda, T.; Abe, H.; Kobayashi, S.; Inaba, K. J. Cry. Pro. Tech. 2014, 4, 193.

(39) Park, J.-H.; Kurosawa, M.; Kawabata, N.; Miyao, M.; Sadoh, T. Electrochem. Sol.-Stat. Lett. 2011, 14, H232.

(40) Park, J.H.; Kasahara. K.; Hamaya. K.; Miyao. M.; Sadoh. T. Appl. Phys. Lett. 2014, 104, 252110.

(41) Sadoh. T.; Park, J.H.; Aoki, R.; Miyao. M. Jpn. J. of Appl. Phys. 2016, 55, 03CB01.

(42) Ba. L.; Qin. Y.; Wu, Z.; J. of Appl. Phys. 1996,80, 6170.

(43) Sugiyama, T.; Mishiba, N.; Kamiko, M.; Kyuno, K. Appl. Phys. Exp. 2016, 9, 095501.

(44) Sharma, R.; Chee, S W.; Herzing, A.; Miranda,R.; Rez, P. Nano Lett. 2011, 11, 2464.

(45) Jin, C B.; Yang, J E.; Joa, M H. Appl. Phys. Lett. 2006, 88, 193105.

(46) Chen, Z G.; Han, G.; Yang, L.; Cheng, L.; Zou, J. Progress in Natural Science: Materials Intl. 2012, 22, 535.

(47) Chueh, Y L.; Boswell, C N.; Yuan, C W.; Shin, S J.; Takei, K.; Ho, J C.; Ko, H.; Fan, Z.; Haller, E E.; Chrzan, D C.; Javey, A. Nano Lett. 2010, 10, 393.

(48) F. A. Ferri, J.Cryst. Sol. 358, (2012), 58.

(49) K. Sakaike, S. Higashi, H. Murakami, and S. Miyazaki, Thi. Sol. Fil. 516, (2008), 3595.

(50) S. M. Sze, Physics of Semiconductor Devices (Wiley, New Jersey, 1936) 2nd ed., p. 20.

(51) H. Takiguchi, Z. Yoshikawa, H. Miyazaki, and Y. Okamoto, J. Electron. Mater. 39, (2010), 1627.

(52) D. G. Cahill, S. K. Watson, and R. O. Pohl, Phys. Rev. B 46, (1992), 6131.

(53) Sadoh, T.; Kurosawa, M.; Hagihara, T.; Toko, K.; Miyao, M.; Electrochemical and Solid-State Letters, 2011, 14, H274.

(54) Uchida, Y.; Funayama, T.; Kogure, Y.; Yeh, W. Jpn. J. of Appl. Phys. 2016, 55, 031303.

(55) Predel B. (2012) Cu - Ge (Copper - Germanium). In: Predel B. (eds) B - Ba … Cu - Zr. Landolt-Börnstein - Group IV Physical Chemistry (Numerical Data and Functional Relationships in Science and Technology), vol 12B. Springer, Berlin, Heidelberg.

(56) Sadoh, T.; Kurosawa, M.; Hagihara, T.; Toko, K.; Miyao, M.; Electrochemical and Solid-State Letters, 2011, 14, H274.

(57) Uchida, Y.; Funayama, T.; Kogure, Y.; Yeh, W. Jpn. J. of Appl. Phys. 2016, 55, 031303.

(58) Toko, K.; Nakazawa, K.;Saitoh, N.; Usami, N.; Suemasu, T. cryst. Growth Des. 2013,13, 3908.

(59) Katsuki, F.; Hanafusa, K.; Yonemura, M.; Koyama, T.; Doi, M. J. Appl. Phys. 2001, 89, 4643.

(60) Zanatta, R.; Chambouleyron, I. J. Appl. Phys. 2005, 97, 094914.

(61) Wang, Z. M.; Wang, J. Y.; Jeurgens, L. P. H.; Phillipp, F.; Mittemeijer, E. J. Acta Mater. 2008, 56, 5047.

(62) Zhang, W.; Ma, F.; Zhang, T.; Xu, K. Thin Solid Films 2011, 520, 708.

(63) Yeh, C. N.; Yang, K.; Lee, H. Y.; Wu, A. T. J. Electron. Mater. 2011, 41, 159.

(64) Chen, Q.; Li, C.; Chen, Z.; Jiao, Z.; Wu, M.; Shek, C.; Wu, C. M. L.; Lai, J. K. L. Inorg. Chem. 2012, 51, 8473.

(65) Peng, S.; Hu, D.; He, D. Appl. Surf. Sci. 2012, 258, 6003.

(66) Nakazawa, K.; Toko, K.; Usami, N.; Suemasu, T. Jpn J of Appl. Phys, 2014, 53, 04EH01.

(67) Toko, K.; Fukata, N.; Nakazawa, K.; Kurosawa, M.; Usami, N.; Miyao, M.; Suemasu, T. J. of Cryst. Grow. 2013,372,189.

(68) McAlister, A.J.; and Murray. J.L.; Bulletin of Alloy Phase Diagrams,1984, 5, 341.

(69) Matsui, M.; Murakami, H.; Fujioka, T.; Ohta, A.; Higashi, S.; Miyazaki, S. Microelectronic Engg. 2011, 88, 1549.

(70) Mori, D.; Oka, H.; Hosoi, T.; Kawai, K.; Morita, M.; Crumlin, E. J.; Liu, Z.; Watanabe, H.; Arima, K. J. App. Phy. 2016, 120, 095306.

(71) Bar, R.; Aluguri, R.; Manna, S.; Ghosh, A.; Satyam, P. V.; Ray, S. K. App. Phy. Lett. 2015, 107, 093102.

(72) Fadida, S.; Eizenberg, M.; Nyns, L.; Van Elshocht, S.; Caymax, M. Microelectronic Engg. 2011, 88, 1557.